THE STABILITY OF FINITE-AMPLITUDE, NEUTRALLY STABLE BAROCLINIC WAVES AND

THEIR ASSOCIATED FRONTS

by

DEAN G. DUFFY

B.S., Case Institute of Technology, 1971

SUBMITTED IN PARTIAL FULFILLMENT OF THE

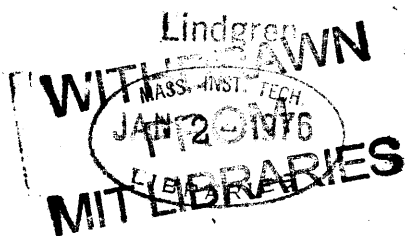REQUIREMENTS FOR THE DEGREE OF DOCTOR OF SCIENCE

at the

MASSACHUSETTS INSTITUTE OF TECHNOLOGY

AUGUST, 1975

Signature of Author ........................................//...........

Department of Meteorology, August 1975

Certified by ...........................................................

Thesis Supervisors

Accepted by ...........................................................

Chairman, Departmental Committee on

Graduate Students

THE STABILITY OF FINITE-AMPLITUDE, NEUTRALLY STABLE BAROCLINIC WAVES AND
THEIR ASSOCIATED FRONTS

by

Dean Gilmore Duffy

Submitted to the Department of Meteorology on 11 August 1975, in partial
fulfillment of the requirements for the degree of Doctor of Science.

## ABSTRACT

Despite the progress made during this century in understanding atmo-
spheric cyclogenesis, frontal cyclogenesis still remains largely an enigma.
This thesis attempts to shed new light on this subject by studying the
stability of a finite-amplitude Eady wave and its associated frontal sur-
face.

By eliminating from consideration at the outset meteorologically un-
important high frequency phenomena, a system of semigeostrophic equations
are derived.  These equations are then transformed into a quasi-Lagrangian
coordinate system which allows a great deal of the nonlinearity to be
eliminated from the problem.

We adopt as our basic state Hoskins and Bretherton's constant potential
vorticity model for describing frontogenesis as a large-scale, finite-
amplitude baroclinic wave in a zonal flow.  It is shown that as a result
of the eddy transports of heat and momentum generated by a growing baro-
clinic disturbance, the zonal available potential energy is reduced
sufficiently so that the finite-amplitude baroclinic wave becomes
neutrally stable.  It is the stability of this neutrally stable, finite-
amplitude baroclinic wave which we will study.

Assuming that the potential vorticity always remains constant, it is
found that this finite-amplitude baroclinic wave is indeed unstable to
further perturbation.  The most unstable perturbations are associated
with length scales of the order of the Rossby radius of deformation,
receive their energy from the available potential and kinetic energy
of the basic state, and move with the speed of the uniform zonal flow.

The distribution of the perturbation's velocity and potential temper-
ature demonstrates that the instabilities are essentially baroclinic in
nature arising from the variations of the potential temperature of the
basic state Eady wave along the boundaries.  The assumption that the
potential vorticity of the basic state is constant inhibits Rayleigh
instability from being a source of instability.

Our analysis suggests, but does not prove, that the major frontal disturbances are essentially baroclinic and that only the smaller scale, fast moving frontal waves are of the Rayleigh type.

Thesis Supervisors:  Jule G. Charney, Peter H. Stone
Titles:  Sloan Professor of Meteorology, Professor of Meteorlogy

# DEDICATION

TO MY PARENTS.

## ACKNOWLEDGEMENTS

TABLE OF CONTENTS

LIST OF FIGURES

## LIST OF TABLES

1. <u>Introduction</u>.

The general circulation of the extratropical zones of the atmosphere is dominated by great migratory vortices (cyclones) traveling in the belt of prevailing westerly winds. During this century, one of the fundamental problems of meteorology has been the explanation of the origin and development of these cyclones.

With the formulation of the polar-front theory of the Norwegian (Bergen) school, J. Bjerknes and Solberg (1922) were able to show that new cyclones may be formed in the crest of amplifying waves on a <u>preexisting</u> polar front. These cyclone waves would then grow in amplitude, occlude, and end as an almost symmetric vortex. To theoretically investigate this model for atmospheric cyclogenesis, Solberg (1928) studied a system consisting of two statically stable, barotropic layers of different density moving zonally at different speeds on a flat, rotating earth. With this basic state, he found two types of amplifying waves were possible: one of short wavelengths of the Helmholtz type and one at wavelengths of the order of 1000 km. The latter possessed several of the kinematic features in common with a young frontal wave.

In the late 1930's, with the ever increasing availability of upper-air data, it was found that the upper-air flow patterns were predominantly large-scale waves embedded in the westerly current with wavelengths of the order of 3000-6000 km. V. Bjerknes (1933) had originally envisioned that cyclones originated as dynamically unstable wavelike disturbances in the westerly current. In 1937 J. Bjerknes (1937) postulated that cyclogenesis could be studied using the concept that the upper-air wave acts as an independent entity. Starting with the tendency equation, Bjerknes

hypothesized that the deepening of cyclones may be attibuted to the rela-

tive displacement of the upper-air wave with respect to the surface

cyclone. Consequently, there should be a one-to-one correspondence

between the surface frontal perturbation and the major perturbation in

the upper atmosphere.

However, subsequent findings based upon improved upper-air observations

failed to verify this one-to-one correspondence. Since the number of

surface frontal perturbations was found to greatly exceed the relatively

small number of major waves and vortices at the upper levels, Charney (1947)

concluded that there was a fundamental difference between the long (3000-

6000 km) waves and the frontal waves of wavelengths 1000-2000 km, although

there was undoubtly a connection between the two types.

Since the late 1940's, Charney (1947) and many others have established

that the origin and development of large-scale extratropical weather

systems result from the baroclinic development of disturbances with the

typical wavelength of several thousand kilometers. However, the expla-

nation of the origin and development of the frontal cyclone, and its

connection with the large-scale baroclinic wave, remains largely an enigma.

Recently, there have been several new attempts to understand these

frontal cyclones. Nitta and Ogura (1972) have numerically simulated the

genesis and development of an intermediate-scale cyclone in a moist model

atmosphere as a result of the finite-amplitude effects of an amplifying,

nonlinear baroclinic wave in a channel flow. Starting with a wave with

a wavelength of 6000 km, the initial disturbance intensified and an

extended front formed. After several days a frontal cyclone formed on

the extended front with a longitudinal wavelength of about 1500 km and

a latitudinal half-wavelength of about 600 km.

One important feature of their model was the inclusion of the latent heat of condensation. When the numerical model lacked a contribution due to moisture, the distribution of the meteorological variables became flater, less distinct, although the broad features remain unchanged.

As an alternative to numerical simulation, Orlanski (1968) has throughly analyzed the instability of a Margules frontal surface (i.e., two incompressible homogeneous fluids with shear and a slight density difference, bounded above and below by two rigid horizontal planes) to further perturbation. He found that the frontal instability combines conventional baroclinic instability with Helmholtz instability and barotropic instabiltty of the Rayleigh type. An important assumption in Orlanski's study of frontal cyclogenesis is that cyclogenesis occurs only <u>after</u> the front has been formed.

Another stability analysis which might be useful in the understanding of frontal cyclogenesis is the study of nongeostrophic baroclinic instability. As was first shown by Stone (1966), nongeostrophic baroclinic instability in the Eady model is a combination of three types of instability which are well known from earlier work; the most unstable modes are associated with conventional baroclinic instability if the Richardson number (Ri) > 0.95, with symmetric instability if 0.95 > Ri > 0.25, and with Kelvin-Helmholtz if Ri < 0.25. In Stone's analysis, there are two growth rate peaks if Ri < 1; one is that of the ordinary baroclinic mode at $\ell$(the meridional wavenumber) = 0 and the other is that of the symmetric instability at k(the zonal wavenumber) = 0, $|\ell| = \infty$.

A distinctive difference between conventional baroclinic instability and symmetric instability is that conventional baroclinic instability draws its energy primarily from the available potential energy of the basic state while the symmetric instability draws its energy primarily from the zonal kinetic energy.

Recently Gambo (1970) and Tokioka (1970,1971) have reinvestigated the nongeostrophic baroclinic problem for the Eady model in the hopes of applying their results to explain frontal cyclogenesis along the "Baiu front" - a persistent phenomenon in the lower atmosphere near Japan or over China during the season of June or July. Upon using parameters representative of a frontal situation, both Gambo (1970) and Tokioka (1971) found that the growth rate peak for the baroclinic mode at $\ell = 0$ when Ri < 1 became a saddle point in the stability diagram (with k as the abscissa and $\ell$ as the ordinate) and a new growth rate peak appeared for small k and a moderate $\ell$. Since the motions associated with this new peak were more rapidly varying in the meridional direction that in the zonal direction, they classified this new growth rate peak as a symmetric instability even though $k \neq 0$. However, if one tries to invoke nongeostrophic baroclinic instability to expalin frontal cyclo-genesis, then one must reconcile the large values of the Richardson number found in the actual atmosphere (normally $\sim 10$) with the small Richardson number needed for the "symmetric" instability of Gambo and Tokioka to become important.

It is the intention of this thesis to study frontal cyclogenesis in a manner different from that of Nitta and Ogura (1972), Orlanski (1968), and Gambo (1970) and Tokioka (1970,1971). It is now well known that

the deformation fields in a developing baroclinic wave produce fronto-
genesis (see Williams,1967). Moreover, once the front has formed, this
frontal surface may itself be unstable to further perturbation.

Recently, analytic expressions for a nonlinear, finite-amplitude Eady
wave which has formed frontal surfaces have been derived by Hoskins and
Bretherton (1972) using the semigeostrophic equations (Eliassen (1949),
Fjørtoft (1962), Hoskins and Bretherton (1972), and Hoskins (1975)) using
a coordinate transformation first introduced by Eliassen (1959). This
immediately suggests that their solutions could be used in an analytic
hydrodynamic stability calculation of a frontal surface created by a
finite-amplitude baroclinic wave embedded in a westerly zonal current.
The resulting stability properties could then be applied to understand
the dynamics of frontal cyclogenesis.

Consequently, it is the purpose of the present investigation to
determine the stability of a finite-amplitude, nonlinear Eady wave
which has generated frontal surfaces to further perturbation. We will
determine the speed of propagation of the disturbances, the exact
stability criteria, and the three-dimensional structure of the most
unstable perturbation. We will then apply these results, as far as
possible, to the study of atmospheric frontal cyclogenesis.

2. Discussion of results.

In this section, the main points will be summarized so that the reader

may have a map of physical insights, unencumbered by mathematical details,

to guide him through the analysis which follows.

Starting with the hydrostatic Boussinesq equations on an f-plane where

all motions take place adiabatically and without friction, the equations

are simplified by neglecting the rate of change of the horizontal ageo-

strophic motions;  the horizontal advecting velocities are, hovever, not

approximated by their geostrophic values.  Since frontal cyclogenesis

takes place on the order of one day (see Nitta and Ogura, 1972), these

semigeostrophic equations should be able to describe frontal cyclo-

genesis without the interference of higher phenemena.

It is now well known that the origin and development of upper-air

waves result from the baroclinic development of large-scale disturbances

with the typical wavelength of several thousand kilometers.  As a result

of the eddy transport of heat and momentum generated by the growing

disturbances, the amount of zonal available potential energy is reduced.

Consequently, although these large-scale disturbances grow initially

according to linear stability theory, sooner or later finite-amplitude

effects will start to slow, and then eventually arrest, the growth of the

baroclinic wave.  Evidence that this feedback process acts strongly in

the atmosphere is shown in Fig 1.

To approximate this observed atmospheric state, our basic state will

consist of a finite-amplitude, neutrally stable Eady wave with no meri-

dional structure embedded in a zonal flow which may possess vertical

shear;  we choose to use the finite-amplitude solutions to the semi-

geostrophic equations found by Hoskins and Bretherton(1972, Section 5).

In our Eady model, this minimization of the zonal available potential energy occurs if we take the zonal shear to be zero. Consequently we shall only consider the case of no zonal vertical shear where the baroclinic wave which has formed a front has the wavelength of the most unstable perturbation from linear stability theory. Fig 2 shows the pressure, temperature, and meridional velocity fields associated with this basic state.

This basic state is then perturbed so that the actual flow is considered to be a small perturbation superimposed on the mean flow. As a first attempt at solving the frontal cyclogenesis problem, we take the potential vorticity to be always constant. Our choice of this constant potential vorticity model has not been made capriciously but has been motivated by the results contained in a paper by Hoskins and Bretherton (1972). In their paper, they obtained frontal models which compared favorably with those observed in the atmosphere by assuming constant potential vorticity. We are trying to extend these constant potential vortictiy models to describe frontal cyclogenesis.

Under the constraint, the linearized perturbation equations are derived. They admit solutions in the form of a sinusoidal wave traveling in the north-south direction with constant speed. The problem which remains is to determine the speed of propagation and the variation of amplitude with height and along a latitude circle as a function of the meridional wavenumber, the amplitude of the Eady wave, and the Rossby number. Since both the velocity and amplitude of the wave may be complex, the wave may grow exponently with time and have a phase shift in the vertical.

The perturbation equations are found to be sufficiently complicated so that they must be solved numerically. This is accomplished by solving the perturbation equations as an initial-value problem (see Brown, 1969). Although this method makes very efficient use of computer storage as well as the computational time needed to calculate the speed of propagation, the noise which is produced upon introducing the arbitary perturbation during the initialization of the numerical scheme results in a complete masking of very small growth rates. Mathematically this noise is assoc-iated with that part of the general solution to the initial-value problem which is not represented by the normal modes (see Pedlosky, 1964).

As an alternative to the numerical solution of the exact perturbation equations, certain nonessential terms are neglected which allow the perturbation equations to be solved analytically. The agreement between the solutions found using the exact and approximate perturbation equations is outstanding.

In Section 6 we examine some of the general stability properties of the perturbation equations using integral methods (see Charney and Stern, 1962). Besides deriving maximum bounds on the growth rates (which is proportional to the product of the meridional wavenumber and the maximum difference in the basic state's velocity) and phase speeds, it is shown that if unstable perturbations exist their instability is a result of the variations of the basic-state potential temperature along the horizontal boundaries. Consequently any instabilities which are found arise from the baroclinic, rather than the barotropic, nature of the basic state.

For any given meridional wavelength, amplitude of the Eady wave, and Rossby number (which do not violate the conditions under which the semi-

geostrophic equations are derived), unstable waves are found.  The most
unstable perturbation is found to be stationary with respect to the
zonal flow, has a characteristic length scale of the Rossby radius
of deformation in both the meridional and zonal direction (NH/f where
N is the Brunt-Vaisalla frequency, H the depth of the Boussinesq atmo-
sphere, and f the constant Coriolis parameter), and receives its energy
from the available potential and kinetic energy of the finite-amplitude
baroclinic wave.

In addition to the unstable stationary perturbations, there are non-
stationary unstable perturbations.  These nonstationary perturbations
have growth rates which are considerably smaller than that for the
stationary perturbation;  consequently, they are of academic interest
only.

In our model, we have taken the potential vorticity of our basic
state to be constant and the potential vorticity of the perturbations
to be zero.  In the case of quasigeostrophic flow, Charney and Stern
(1962) have shown that there are two possible sources of instability
in a baroclinic-barotropic circumpolar vortex.  One of the sources
of instability is the variations of the potential temperature along
the horizontal boundaries.  We have this type of instability in our
model and it is associated with conventional baroclinic instability.
Another source of instability is due to the vanishing of the meridional
derivative of the potential vorticity in an isoentropic surface or the
pseudopotential vorticity in a level surface somewhere within the
flow.  In our problem, this would correspond to a vanishing of the
meridional derivative of the basic state's potential vorticity some-
where within the flow.  This does not occur in our problem and has

the consequence of excluding Rayleigh instability in the flow.

Our results are in qualitative agreement with those of Orlanski(1968) if the Rossby number is sufficiently small and the Richardson number is sufficiently large so that the semigeostrophic equations are valid. The most unstable perturbation has a length scale along the front of the order of the Rossby radius of deformation and receives its energy from both the basic state's available potential and kinetic energy. The most unstable perturbation does not, however, move with the mean zonal flow.

In Section 9 we display the pressure, temperature, total velocity, and perturbation's relative vorticity fields for the most unstable perturbation. As expected of a baroclinic-like instability, warm air rises and spreads out in the upper levels while cold air sinks and spreads out in the lower levels. In this manner, the temperature contrast across the frontal surfaces is destroyed.

As an application of the results found in our stability analysis, we examine the development of a frontal cyclone over the midwestern United States in Section 10. Although a detailed comparison shows marked differences between our model and the observed situation, the overall, smoothed temperature, pressure, and vertical velocity fields are explained.

Thus, our analysis suggests but does not prove that the major frontal disturbances are essentially baroclinic instabilities and that only the smaller scale, fast moving frontal waves are of the Rayleigh type.

3. <u>The</u> <u>governing</u> <u>equations</u>.

In this paper we will employ the Boussinesq equations, bounding the domain with two rigid horizontal planes. The compressibility of the atmosphere, which is neglected in the Boussinesq approximation, may be shown to be qualitatively unimportant in the case of atmospheric frontogenesis since the density scale height of the atmosphere is much larger than the thickness of typical frontal zones. In addition, Nitta and Ogura (1972) have found that an intermediate-scale cyclone is most pronounced in the region below 700 mb, indicating that it too should be relatively unaffected by compressibility. The replacement of the tropopause by a rigid horizontal surface can be expected to give large errors in that region, but the resulting errors near the bottom boundary, the region that will be of greatest interest for us, should be small.

We shall also employ the hydrostatic approximation. Since the horizontal scale during frontogenesis and frontal cyclogenesis remains much larger than the vertical scales, the hydrostatic balance should be valid throughout the entire field of motion.

Approximating the spherical geometry of the earth with a Cartesian tangent plane, we denote the eastward, northward and vertically upward Cartesian coordinates by $x'$, $y'$, and $z'$; their corresponding velocities by $u'$, $v'$, and $w'$; time by $t'$; the constant Coriolis parameter by $f$; the departure of the potential temperature $\theta_0$, a constant reference potential temperature, by $\theta'$; the pressure function by $\phi'$; and the acceleration due to gravity by $g$. The hydrostatic Boussinesq equations can be written in the following form:

$$u'_{t'} + u'u'_{x'} + v'u'_{y'} + w'u'_{z'} + \phi'_{x'} - fv' = 0 \qquad (3.1)$$

$$v'_{t'} + u'v'_{x'} + v'v'_{y'} + w'v'_{z'} + \phi'_{y'} + fu' = 0 \qquad (3.2)$$

$$\phi'_{z'} - g\theta'/\theta_0 = 0 \qquad (3.3)$$

$$u'_{x'} + v'_{y'} + w'_{z'} = 0 \qquad (3.4)$$

$$\theta'_{t'} + u'\theta'_{x'} + v'\theta'_{y'} + w'\theta'_{z'} = 0 \qquad (3.5)$$

where
$$\kappa = R/C_p,$$

$$\theta' = T(p_0/p)^\kappa - \theta_0, \qquad (3.6)$$

$$\phi' = C_p\theta_0(p/p_0)^\kappa + gz', \qquad (3.7)$$

T the absolute temperature of the fluid, R the (ideal) gas constant, $C_p$ the specific heat at constant pressure, p the pressure of the fluid, and $p_0$ a constant reference pressure. The subscripts in x',y',z', and t' denote partial differentiations.

Two physical processes which have been neglected in (3.1)-(3.5) are heating and friction. In their study, Nitta and Ogura (1972) included the eddy diffusion of momentum, heat, and water vapor as well as surface friction, evaporation, and the release of latent heat of condensation. Of all of these above effects, they found that the release of latent heat of condensation to be most important. At present, we shall neglect this effect. Any scheme for the inclusion of the latent heat of condensation into our problem, except for a simplistic modification of the atmosphere's static stability, would make the problem analytically untractable. From previous studies, however, we should anticipate that the effects of condensation would tend to intensify the instability of the system as well as reduce the scale of the disturbance (Nitta, 1964).

The boundary conditions are

$$w' = 0 \qquad \text{at } z' = 0, H,$$

where H is the distance between the horizontal plates. The boundary conditions in the zonal and meridional directions will be specified later.

Let L denote the characteristic length scale, U a characteristic horizontal velocity scale, H the distance between the two horizontal plates, L/U the advective time scale, then we may nondimensionalize (3.1)-(3.5) as follows;

$$(x,y) = (x',y')/L; \quad z = z'/H; \quad (u,v) = (u',v')/U; \quad w = Lw'/UD; \quad t = Ut'/L;$$

$$\phi = \phi'/fUL; \quad \text{and} \quad \theta = gH\theta'/\theta_0 fUL$$

$$Ro(u_t + uu_x + vu_y + wu_z) + \phi_x - v = 0 \tag{3.8}$$

$$Ro(v_t + uv_x + vv_y + wv_z) + \phi_y + u = 0 \tag{3.9}$$

$$\phi_z - \theta = 0 \tag{3.10}$$

$$u_x + v_y + w_z = 0 \tag{3.11}$$

$$\theta_t + u\theta_x + v\theta_y + w\theta_z = 0 \tag{3.12}$$

where Ro is the Rossby number, Ro = U/fL. Eqs (3.10) and (3.12) can be combined to yield

$$\phi_{zt} + u\phi_{zx} + v\phi_{zy} + w\phi_{zz} = 0 \tag{3.13}$$

with the boundary conditions w = 0 at z = 0,1.


## 3.1. The semigeostrophic equations.

Eqs (3.8), (3.9), (3.11), and (3.13) are still too general for our use; not only do they describe frontogenesis and frontal cyclogenesis but also gravity wave motions. From the study of Hoskins and Bretherton (1972), we know that gravity waves are of negligible importance in the description of frontogenesis; from a diagnostic study of a developing wave cyclone, Krishnamurti (1968) has demonstrated that the balance equations may be used to accurately describe the development of a wave cyclone. Since

neglecting gravity motions results in considerable simplification of the analysis that is to follow, we shall introduce a system of semigeostrophic equations which were first derived by Eliassen (1949) and later rederived by Fjortoft (1962) and Hoskins (1975).

We rewrite (3.8)-(3.9) as

$$v = \phi_x + Ro(u_t + uu_x + vu_y + wu_z) \tag{3.14}$$

$$u = -\phi_y - Ro(v_t + uv_x + vv_y + wv_z) \tag{3.15}$$

We now substitute (3.15) into the substantial derivative in (3.14) and substitute (3.14) into the substantial derivative in (3.15) and obtain

$$v = v_g + Ro\frac{Du_g}{Dt} - Ro^2\frac{D^2v}{Dt^2} \tag{3.16}$$

$$u = u_g - Ro\frac{Dv_g}{Dt} - Ro^2\frac{D^2u}{Dt^2} \tag{3.17}$$

where

$$\frac{D}{Dt} = \frac{\partial}{\partial t} + u\frac{\partial}{\partial x} + v\frac{\partial}{\partial y} + w\frac{\partial}{\partial z}$$

$$v_g = \phi_x$$

and

$$u_g = -\phi_y.$$

Upon repeated substitution of (3.14)-(3.15) into the substantial derivatives (in the same manner as above) to replace $v$ and $u$, respectively, we may replace (3.14)-(3.15) with the power series:

$$v = \sum_{n=0}^{\infty} (-1)^n Ro^{2n} \frac{D^{2n}}{Dt^{2n}}\{v_g + Ro\frac{D}{Dt}(u_g)\} \tag{3.18}$$

$$u = \sum_{n=0}^{\infty} (-1)^n Ro^{2n} \frac{D^{2n}}{Dt^{2n}}\{u_g - Ro\frac{D}{Dt}(v_g)\} \tag{3.19}$$

The essence of the semigeostrophic equations is to truncate (3.18)-(3.19) at $n = 0$, so that

$$Ro(u_{gt} + uu_{gx} + vu_{gy} + wu_{gz}) + v_g - v = 0 \tag{3.20}$$

$$Ro(v_{g_t} + uv_{g_x} + vv_{g_y} + wv_{g_z}) - u_g + u = 0 \tag{3.21}$$

Eqs (3.20)-(3.21) will be a good approximation to (3.18)-(3.19) when the remaining terms of (3.18)-(3.19) are small compared to the n = 0 term. For well-behaved expressions for $\phi$ (i.e., expressions whose derivatives do __not__ become large as the order of the derivatives is increased), the semigeostrophic equations (3.18)-(3.19) are clearly valid if

$$Ro^2 \left| \frac{D^2}{Dt^2}(v_g + Ro\frac{Du_g}{Dt}) \right| / \left| v_g + Ro\frac{Du_g}{Dt} \right| \ll 1 \tag{3.22}$$

and

$$Ro^2 \left| \frac{D^2}{Dt^2}(u_g - Ro\frac{Dv_g}{Dt}) \right| / \left| u_g - Ro\frac{Dv_g}{Dt} \right| \ll 1. \tag{3.23}$$

The inequality in (3.22) and (3.23) might be violated if the denominator vanishes. Although this might occur in a small region of the flow field (when $v_g$ and $u_g$ change sign, for example), this would indicate that the semigeostrophic equations were giving locally poor results but the remaining portions of the flow field might be described very accurately. Consequently, in using (3.22)-(3.23) to test the validity of the semigeostrophic equations to the whole flow field, a global view of how well (3.22)-(3.23) is being satisfied is needed.

The central difference between our set of semigeostrophic equations (3.20)-(3.21) and the quasigeostrophic equations is the retention of the ageostrophic horizontal advection. As Hoskins (1975) has pointed out, this is entirely analogous to the hydrostatic approximation in which the vertical component of momentum is neglected but vertical velocity is retained in the substantial derivative and continuity equation.

Besides simplifying the set of governing equations, the semigeostrophic equations possess the following set of conservation laws:

(1) conservation of potential temperature;

$$\frac{D}{Dt}(\phi_z) = 0 \qquad (3.24)$$

(2) conservation of vorticity

$$\frac{D}{Dt}(\underline{\zeta}_g) = (\underline{\zeta}_g \cdot \underline{\nabla}_3)\underline{u} - \underline{k} \times \underline{\nabla}_3 \theta \qquad (3.25)$$

(3) conservation of potential vorticity

$$\frac{D}{Dt}(q_g) = 0 \qquad (3.26)$$

and (4) the energy equation

$$\frac{D}{Dt}(K_g + P) = -\underline{\nabla}_3 \cdot (\underline{u}\phi) \qquad (3.27)$$

where

$$\underline{\zeta}_g = (-Ro\phi_{xz} + Ro^2(-\phi_{yy}\phi_{xz} + \phi_{yz}\phi_{xy}), \ -Ro\phi_{yz} + Ro^2(-\phi_{yz}\phi_{xx} + \phi_{xy}\phi_{xz}),$$

$$1 + Ro(\phi_{xx} + \phi_{yy}) + Ro^2(-\phi_{xy}^2 + \phi_{xx}\phi_{yy})) \qquad (3.28)$$

$$q_g = \underline{\zeta}_g \cdot \underline{\nabla}_3 \theta \qquad (3.29)$$

$$K_g = \tfrac{1}{2}Ro(\phi_x^2 + \phi_y^2)$$

and $\qquad P = -z\theta.$

All of the above equations have been derived from (3.11), (3.13), (3.20), and (3.31).


## 3.2. The Eliassen coordinate.

Despite the fact that (3.11), (3.12), (3.20), (3.21) are simpler than the primitive equations, they still have not been brought into their simplest form. This subsection is devoted to the derivation of a co-ordinate transformation which results in such an amazing simplification of the semigeostrophic equations that many of the results, which would

normally be amendable only through numerical calculations, can be derived analytically.

To begin the analysis, we define four new independent variables, first introduced by Eliassen (1959), as follows:

$$X = x + Ro\ \phi_x, \quad Y = y + Ro\ \phi_y, \quad Z = z, \quad T = t. \tag{3.30}$$

Since
$$\frac{DX}{Dt} = u_g \text{ and } \frac{DY}{Dt} = v_g,$$

Hoskins and Bretherton (1972) have referred to them as geostrophic co-ordinates since they represent the positions particles would have had if they had moved with their geostrophic velocity at every instant instead of their actual velocity. We shall refer to these new coordinates however as the Eliassen coordinates.

Upon performing the transformation, we find that the Jacobian of the transformation is

$$J = \underline{k} \cdot \underline{\zeta}_g = \frac{\partial(X,Y)}{\partial(x,y)} \tag{3.31}$$

as well as
$$J \frac{\partial}{\partial Z} = \underline{\zeta}_g \cdot \underline{\nabla}_3$$

where $\underline{\zeta}_g$ is defined by (3.28).

If we now define

$$\Phi = \phi + \tfrac{1}{2}Ro(\phi_x^2 + \phi_y^2), \tag{3.32}$$

it is easily verified that

$$(\Phi_X, \Phi_Y, \Phi_Z) = (\phi_x, \phi_y, \phi_z). \tag{3.33}$$

Using (3.31) and the transformation equation, we find that

$$J^{-1} = 1 - Ro(\Phi_{XX} + \Phi_{YY}) + Ro^2(\Phi_{XX}\Phi_{YY} - \Phi_{XY}^2). \tag{3.33}$$

Having performed the coordinate transformation, we are prepared to derive the conservation equations in the Eliassen coordinates. From

(3.31) we have

$$J \frac{\partial \theta}{\partial Z} = \underline{\zeta}_g \cdot \underline{\nabla}_3 \theta = q_g \tag{3.35}$$

Therefore,

$$\frac{1}{q_g} \Phi_{ZZ} + Ro(\Phi_{XX} + \Phi_{YY}) - Ro^2(\Phi_{XX}\Phi_{YY} - \Phi_{XY}^2) = 1 \tag{3.36}$$

since $\theta = \partial \Phi / \partial Z$.

Turning our attention to the material time derivative, we find that following a fluid particle

$$\frac{D}{Dt} = \frac{D}{DT} = \frac{\partial}{\partial T} - \Phi_Y \frac{\partial}{\partial X} + \Phi_X \frac{\partial}{\partial Y} + w \frac{\partial}{\partial Z} \tag{3.37}$$

so that conservation of potential temperature and vorticity becomes

$$\frac{D}{Dt}(\Phi_Z) = 0 \tag{3.38}$$

and

$$\frac{D}{Dt}(q_g) = 0. \tag{3.39}$$

From (3.38) we find that the boundary conditions along the boundaries are

$$\left( \frac{\partial}{\partial T} - \Phi_Y \frac{\partial}{\partial X} + \Phi_X \frac{\partial}{\partial Y} \right) \Phi_Z = 0 \tag{3.40}$$

on $Z = 0,1$.

Having introduced the Eliassen coordinates, we have mapped the semigeostrophic equations into a form which is very similar to that of the quasigeostrophic equations. Consequently, many of the known solutions to the quasigeostrophic equations may be used to solve the semigeostrophic equations with only a distortion of the solution due to the coordinate transformation. This distortion is vital however in the description of frontogenesis and frontal cyclogenesis. The difficulty with this coordinate system is that it is a quasi-Lagrangian system where we must make a highly nonlinear transformation to get back into physical space.

However, this may be accomplished graphically, a small price to pay for

having made the equations which govern the nonlinear flows of fronto-

genesis and frontal cyclogenesis nearly linear.

3.3.  The constant potential vorticity model.

With the derivation of (3.36), (3.38), (3.39), and (3.40), the semi-

geostrophic equations (3.24)-(3.29) have been transformed into the Eliassen

coordinate system <u>without</u> <u>approximation</u>.  We shall presently place a re-

striction on the semigeostrophic equations which will allow us to con-

struct a model of frontal cyclogenesis without a cumbersome mathematical

treatment, namely, that the <u>potential</u> <u>vorticity</u> as defined by (3.35) <u>is</u>

<u>always</u> <u>constant</u>.  With this simplifying assumption, the vertical velocity

does not appear explicitly in the governing equations.  Since this as-

sumption saves us from solving a vertical velocity equation, the problem

may be attacked primarily by analytical techniques rather than as a

numerical experiment.

Our choice of this constant potential vorticity model has not been made

capriciously but has been motivated by the results contained in a paper by

Hoskins and Bretherton (1972).  In their paper, they obtained frontal

models which compared favorably with those observed in the atmosphere by

assuming constant potential vorticity.  We are trying to extend these

constant potential vorticity models to describe frontal cyclogenesss.

To reduce the parameters in our analysis, we shall take our character-

istic length scale L to equal the Rossby radius of deformation (NH/f where

N is the Brunt-Väisalla frequency).  We further take the constant potential

vorticity to equal $Ro^{-1}$, and substract out the mean atmospheric stratifi-

cation by introducing $\psi$ so that $\psi = \Phi - \frac{1}{2}RoZ^2$. $\qquad\qquad$ (3.41)

The governing equations now become

$$\psi_{ZZ} + \psi_{XX} + \psi_{YY} - Ro\psi_{XX}\psi_{YY} + Ro\psi_{XY}^2 = 0 \qquad\qquad (3.42)$$

and

$$\left(\frac{\partial}{\partial T} - \psi_Y \frac{\partial}{\partial X} + \psi_X \frac{\partial}{\partial Y}\right)\psi_Z = 0 \qquad\qquad (3.43)$$

along $Z = 0,1$. For the remaining portions of this thesis, we shall use (3.42) and (3.43) to study frontal cyclogenesis.

4. The basic state: the unperturbed finite-amplitude wave and its associated front.

To begin our discussion of the basic state, we shall take a uniform zonal flow which may possess constant vertical shear plus an Eady wave without any meridional structure:

$$\bar{\psi} = - Y - \delta(Z-1/2)Y + \psi^{(E)}(X,Z,T) \qquad (4.1)$$

where $\delta$ is a measure of the vertical shear and $\epsilon$ the amplitude of the Eady wave. By translating the coordinate system with the speed of the zonal flow at the mid-level, we may stbtract out the constant zonal flow by making the substitution $X_0 = X - T$.

Substituting (4.1) into (3.42)-(3.43) we find that $\psi^{(E)}$ is governed by

$$\psi^{(E)}_{ZZ} + \psi^{(E)}_{X_0 X_0} = 0 \qquad (4.2)$$

subject to the boundary condition along $Z = 0,1$

$$(\frac{\partial}{\partial T} + \delta(Z-1/2)\frac{\partial}{\partial X_0})\psi^{(E)}_Z - \delta\, \psi^{(E)}_{X_0} = 0 \qquad (4.3)$$

The solution to (4.2) is

$$\psi^{(E)} = \exp(\sigma\delta T)(A \cosh k(Z-1/2) \cos kX_0 + B \sinh k(Z-1/2) \sin kX_0) \qquad (4.4)$$

with $$\sigma^2 = (x-\coth(x))(\tanh(x)-x) \qquad (4.5)$$

where $$x = k/2$$

and $$\sigma A = B(1 - x \coth(x))$$

$$\sigma B = A(x \tanh(x) - 1).$$

To complete our derivation of the basic state, we must now choose those values of $\delta$ and $k$ that best approximate finite-amplitude baroclinic waves as they exist in the atmosphere.
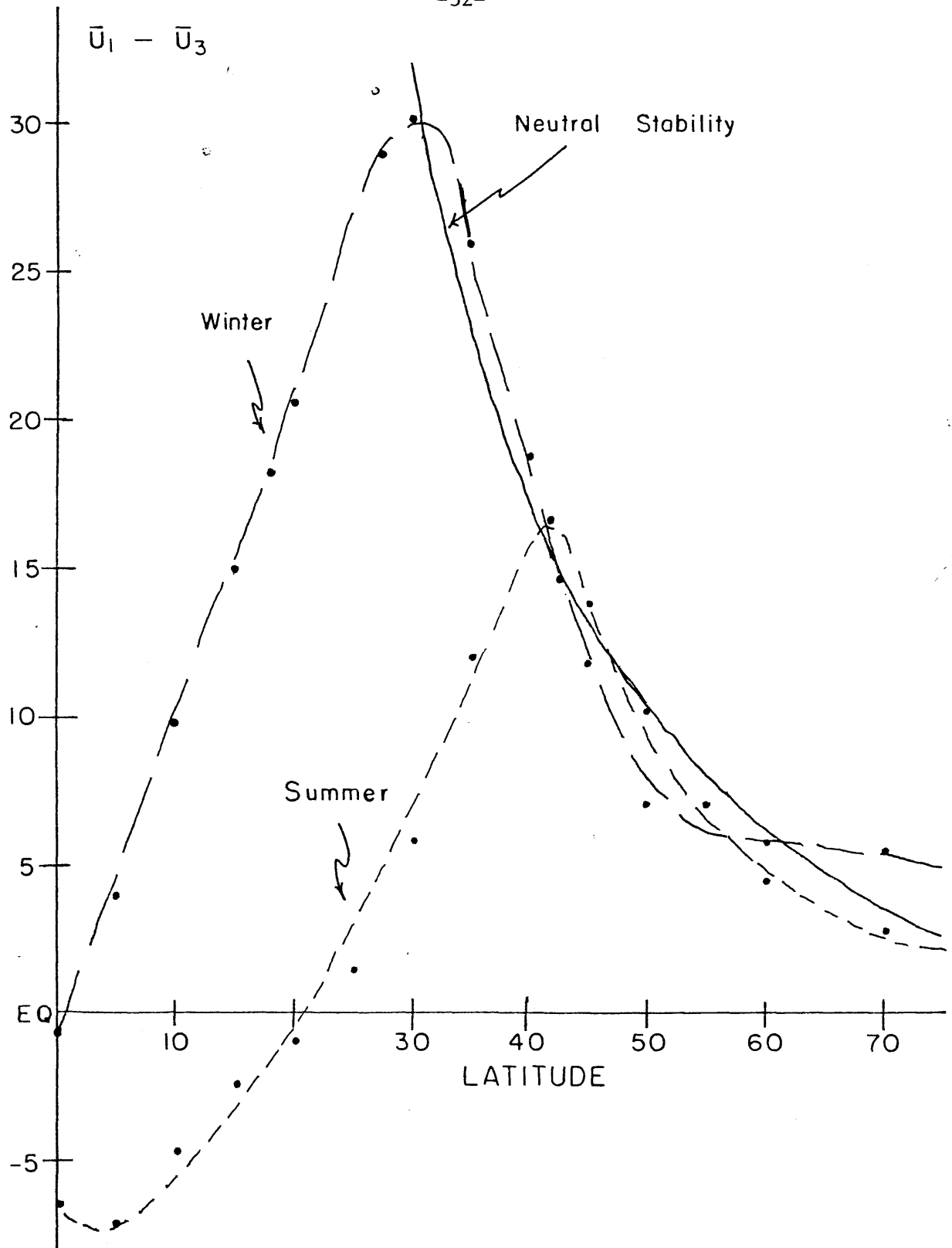
Fig 1. The shear profiles from the local baroclinic stability criterion, $\bar{U}_{200} - \bar{U}_{700} = 4\Omega aS \cos(\text{lat.})/\sin^2(\text{lat.})$ for $S = 0.005$ and the observed mean summer and winter values of $\bar{U}(200\text{mb}) - \bar{U}(700\text{mb})$ (Oort and Rasmusson, 1971).

It is now well known that the origin and development of upper-air

waves result from the baroclinic development of disturbances with the

typical wavelength of several thousand kilometers. As a result of the

eddy transports of heat and momentum generated by the growing dis-

turbances, the zonal available potential energy is reduced. Consequently,

although these large-scale disturbances grow initially according to

linear stability theory, sooner or later finite-amplitude effects will

start to slow, and then eventually arrest, the growth of the baroclinic

wave.

Evidence that this feedback process acts strongly in the atmosphere

is shown in Fig 1 which compares the observed zonal shear from summer

and winter (Oort and Rasmusson, 1971) with the zonal shear from the

local baroclinic instability criterion derived from a two-level,

β-plane model:

$$\bar{U}_1 - \bar{U}_3 \geq 4\Omega aS \cos(\text{lat.})/\sin(\text{lat.})$$

where $\Omega$ and a are the angular velocity and radius of the earth, and

S the nondimensional static stability of the atmosphere (Phillips, 1954).

The observed vertical shear is computed by differencing observed

seasonal values of $\bar{U}$ at 200 mb and 700 mb. Fig 1 suggests that the

observed, finite-amplitude baroclinic waves in the extratropical regions

of the atmosphere limit the zonal available potential energy to such

a degree that it does not greatly exceed the amount necessary for

instability.

In our Eady model, the flow is unstable for any vertical shear of

the zonal flow; hence, the consistent minimization of the zonal

available potential energy occurs for zero zonal shear. Consequently,

from this point forward, we shall take $\delta = 0$. Furthermore, since there

is no physical reason why wavelengths other than that associated with the most unstable Eady mode as found from linear stability theory (i.e., $k = 1.6062$) should be excited, we shall also use that value of $k$ in our analysis. Although the finite-amplitude effects have probably changed it from its original value, this value is certainly near the correct one. Also B will have the same relation to A as in the case of the most unstable Eady wave.

Using (4.1), (3.20), (3.21), and (3.13), we find that the basic state consists of

$$\bar{\theta} = \bar{\psi}_Z = Ro^{-1}(Z-1/2) + \varepsilon Ak \sinh k(Z-1/2) \cos kX_0 +$$
$$+ \varepsilon Bk \cosh k(Z-1/2) \sin kX_0 \qquad (4.6)$$

$$\bar{w} = 0$$

$$\bar{u} = 1 \qquad (4.7)$$

$$\bar{v} = \bar{v}_g = -\varepsilon Ak \cosh k(Z-1/2) \sin kX_0 + \varepsilon Bk \sinh k(Z-1/2) \cos kX_0 \qquad (4.8)$$

Fig 2 shows vertical cross sections of $\bar{\theta}^{(E)}$ (i.e., the temperature field with the mean stratification subtracted out), $\bar{v}$ at $y = 0$ in the un-stretched coordinates, and $\bar{\phi}$ at $z = 1/2$ (corresponding to 500 mb) when $\varepsilon kRo = 0.4$. Since the magnitude of $\bar{v}$ is associated with $\varepsilon$; A may be taken to equal one without any loss of generality.

In certain respects, the case of no zonal shear is a generalization of Orlanski's model. Instead of a discontinuity for a front, we have continuous variations of temperature and vorticity. Also the properties of the front are directly associated with the finite-amplitude baroclinic wave that produced it. Finally, we also have vertical and horizontal shear across the front, as Orlanski's model does, without any temperature variations along the front.
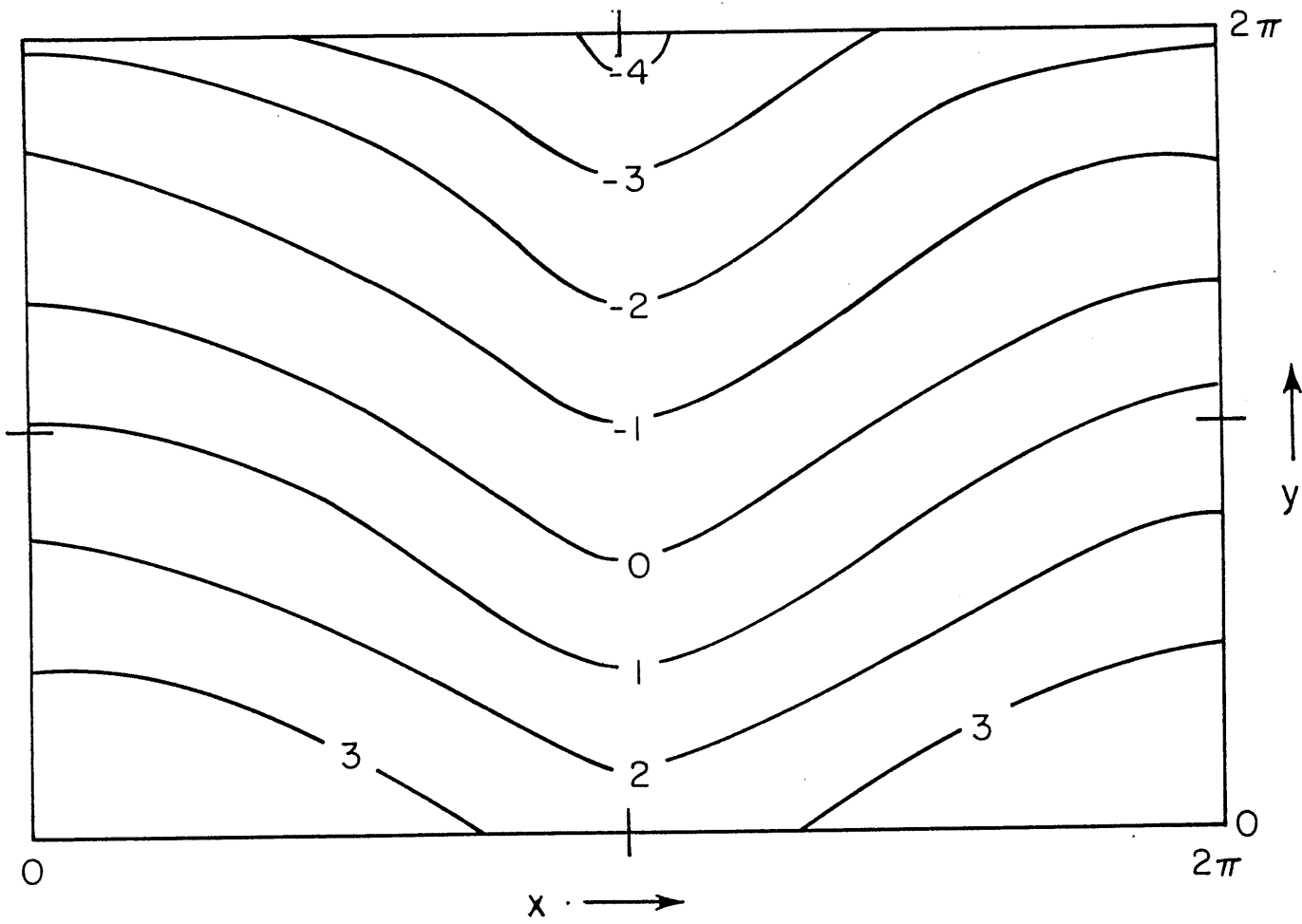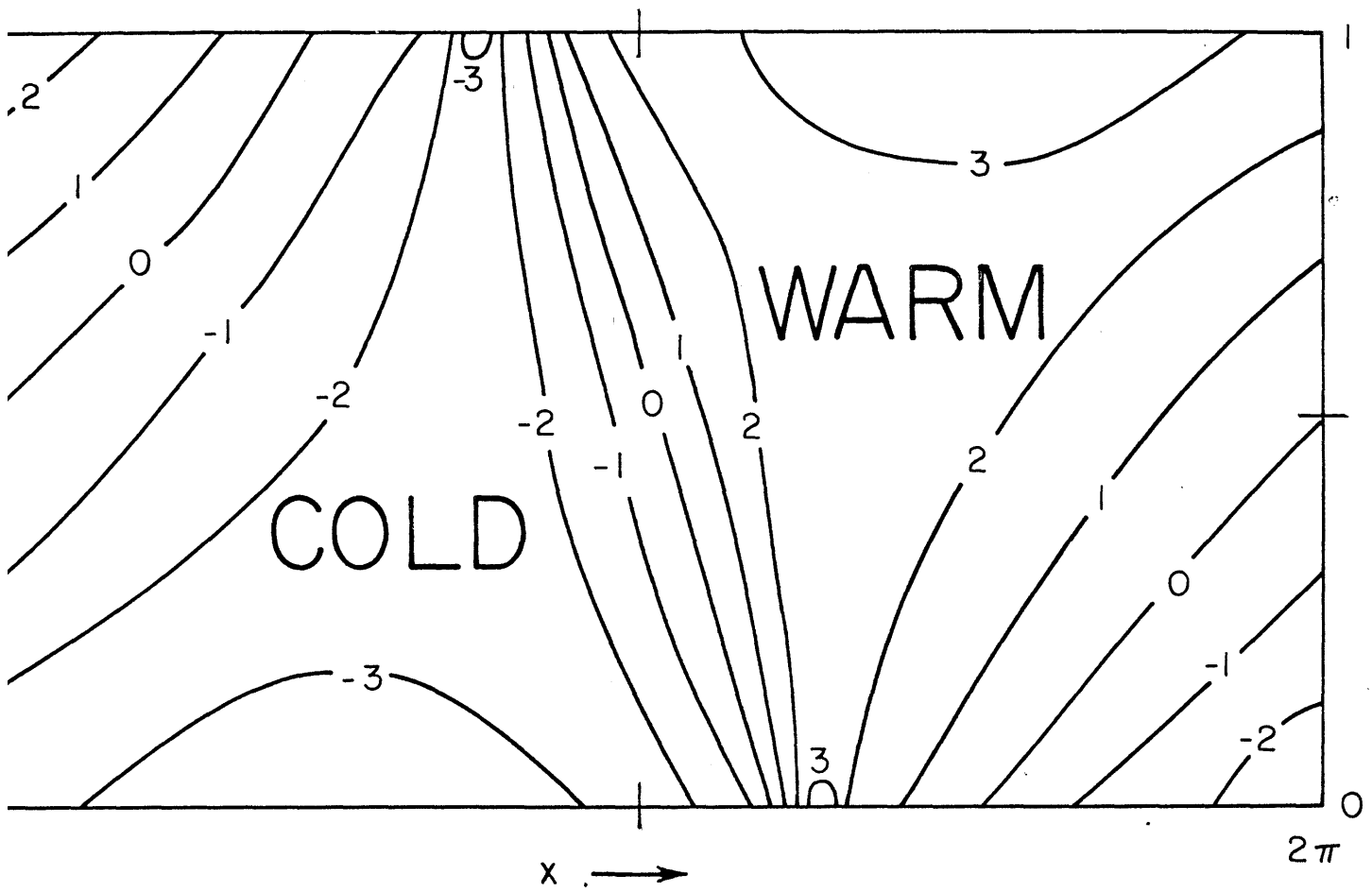
Fig 2.1.   The basic state's pressure field at z = 1/2.

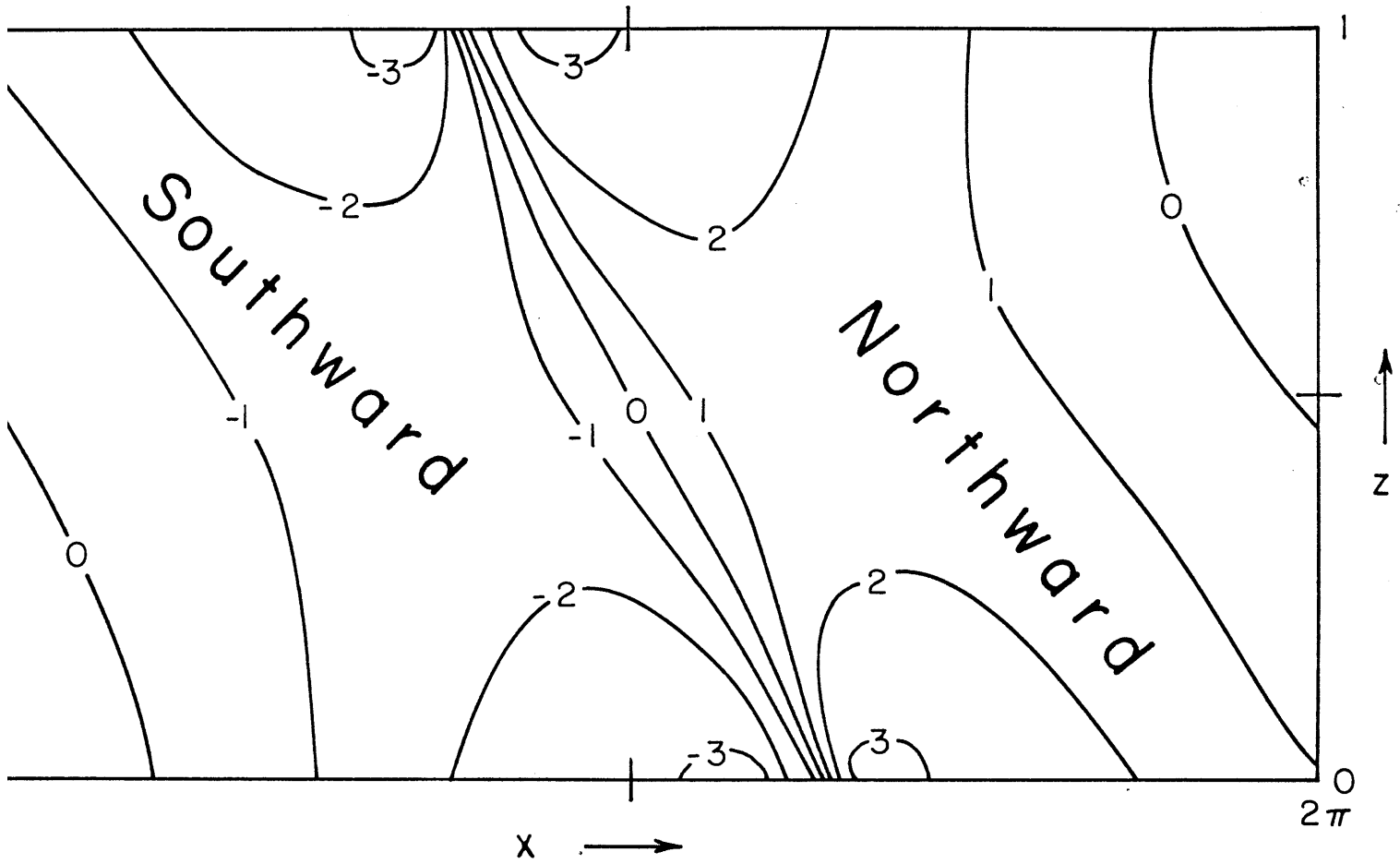Fig 2.2.   The potential temperature field of the Eady wave at y = 0.

Fig 2.3.   The basic state's meridional velocity field at y = 0.

As a point of departure, we do not have a discontinuity of potential vorticity as dows Orlanski's model at his frontal surface. We will return to this point later.

Finally we must test (4.6)-(4.8) to see when the semigeostrophic equations break down according to (3.22)-(3.23). Since $D^n\bar{v}/Dt^n = D^n\bar{u}/Dt^n = 0$ when $n \leq 1$ and $D/Dt = \partial/\partial T + \bar{u}_g \, \partial/\partial X + \bar{v}_g \, \partial/\partial Y + \bar{w} \, \partial/\partial Z$, then (3.22)-(3.23) is satisfied for all $\varepsilon$, $k$, and Ro. However, since the vertical component of the basic state's absolute vorticity (which is equal to $(1-\varepsilon Ro\psi_{X_0 X_0}^{(E)})^{-1}$) must remain finite, it is found that in reality $\varepsilon k Ro \leq 0.4$.

## 5. Perturbation equations.

### 5.1. The linearized equations.

We now consider that the actual flow is a small perturbation super-imposed on the steady flow described in Section 4. Thus,

$$\psi = \overline{\psi} + \psi'$$

$$w = w'$$

$$(5.1)$$

Substituting the perturbed $\psi$ and $w$ into (3.42)-(3.43), subtracting out the basic state, and neglecting quadratic perturbation terms, we obtain the system

$$\psi'_{ZZ} + \psi'_{X_0 X_0} + \psi'_{YY} - \varepsilon Ro \psi^{(E)}_{X_0 X_0} \psi'_{YY} = 0 \qquad (5.2)$$

and

$$\left( \frac{\partial}{\partial T} + \varepsilon \psi^{(E)}_{X_0} \frac{\partial}{\partial Y} \right) \psi'_Z - \varepsilon \psi^{(E)}_{X_0 Z} \psi'_Y = 0 \qquad (5.3)$$

Since $\psi^{(E)}$ is independent of $Y,T$ we may assume that $\psi'$ varies as $\exp(i\ell Y + i\lambda T)$ where $\ell$ is the (real) meridional wavenumber and $\lambda$ may be complex. If $\lambda_i = \text{Im}(\lambda) < 0$, then we have found an unstable mode for the given value of $\varepsilon$, $\ell$, Ro. Assuming that

$$\psi' \sim \Psi(X_0, Z) \exp(i\ell Y + i\lambda T) \qquad (5.4)$$

then (5.2)-(5.3) becomes

$$\Psi_{ZZ} + \Psi_{X_0 X_0} - \ell^2 \Psi + \varepsilon Ro \ell^2 \psi^{(E)}_{X_0 X_0} \Psi = 0 \qquad (5.5)$$

and

$$\lambda \Psi_Z + \varepsilon \ell \psi^{(E)}_{X_0} \Psi_Z - \varepsilon \ell \psi^{(E)}_{X_0 Z} \Psi = 0 \qquad (5.6)$$

The $X_0, Z$ dependence of $\psi^{(E)}$ is rather complicated. The simplest solution to (5.5)-(5.6) which takes the sinusoidal $X_0$ dependence of the baroclinic wave into account assumes the form of

$$\Psi = \sum_{n = -\infty}^{\infty} \Psi^{(n)}(Z) \exp(inkX_0 + ik_0 X_0) \qquad (5.7)$$

where $k_0$ is any arbitary zonal wavenumber. For the present study, we shall restrict ourselves to $k_0 = 0$. The most general solution to (5.5)-(5.6) would, of course, require that the $k_0 = 0$ condition would have to be relaxed.

Upon substituting (5.7) into (5.5)-(5.6), we obtain the following set of ordinary differential equations:

$$\Psi_{ZZ}^{(n)} - n^2 k^2 \Psi^{(n)} - \ell^2 \Psi^{(n)} = \varepsilon Ro k^2 \ell^2 A_{n-1} \Psi^{(n-1)} + \varepsilon Ro k^2 \ell^2 A_{n+1} \Psi^{(n+1)} \quad (5.8)$$

and

$$i\lambda \Psi_Z^{(n)} + \varepsilon k\ell B_{n+1} \Psi^{(n+1)} + \varepsilon k\ell B_{n-1} \Psi^{(n-1)} + \varepsilon k\ell C_{n+1} \Psi_Z^{(n+1)} + \varepsilon k\ell C_{n-1} \Psi_Z^{(n-1)} = 0 \quad (5.9)$$

along $Z = 0,1$ where

$$A_{n+1} = \tfrac{1}{2} A \cosh k(Z-\tfrac{1}{2}) + \tfrac{1}{2}i B \sinh k(Z-\tfrac{1}{2})$$

$$A_{n-1} = \tfrac{1}{2} A \cosh k(Z-\tfrac{1}{2}) - \tfrac{1}{2}i B \sinh k(Z-\tfrac{1}{2})$$

$$B_{n+1} = -\tfrac{1}{2}ik B \cosh k(Z-\tfrac{1}{2}) - \tfrac{1}{2}k A \sinh k(Z-\tfrac{1}{2})$$

$$B_{n-1} = -\tfrac{1}{2}ik B \cosh k(Z-\tfrac{1}{2}) + \tfrac{1}{2}k A \sinh k(Z-\tfrac{1}{2})$$

$$C_{n+1} = \tfrac{1}{2}i B \sinh k(Z-\tfrac{1}{2}) + \tfrac{1}{2} A \cosh k(Z-\tfrac{1}{2})$$

and

$$C_{n-1} = \tfrac{1}{2}i B \sinh k(Z-\tfrac{1}{2}) - \tfrac{1}{2} A \cosh k(Z-\tfrac{1}{2})$$

Due to the complicated form of $A_{n+1}$ and $A_{n-1}$, a general analytic solution to (5.8) cannot be found which could then be substituted into (5.9) to find $\lambda$. Therefore, we must solve (5.8)-(5.9) numerically.

Instead of solving (5.8)-(5.9) in the manner suggested by Orlanski (1968), (5.9) is rewritten

$$\Psi_{ZT}^{(n)} + \varepsilon k\ell B_{n+1} \Psi^{(n+1)} + \varepsilon k\ell B_{n-1} \Psi^{(n-1)} + \varepsilon k\ell C_{n+1} \Psi_Z^{(n+1)} + \varepsilon k\ell C_{n-1} \Psi_Z^{(n-1)} = 0 \quad (5.10)$$

and (5.8) and (5.10) are solved as an initial-value problem.

## 5.2. The numerical technique.

The numerical technique employed in the present investigation to obtain the linear solutions to (5.8) and (5.10) is one of an initial-value type. The major advantage of this method is the compactness of the computer memory necessary for large vertical resolution; the major disadvantage is the presence of background noise due to the initialization scheme.

For a given Rossby number, meridional wavenumber, amplitude of the Eady wave, and basic state zonal wavenumber, an initial perturbation $\psi_Z^{(n)}$ is generated by a random number generator along the upper and lower boundaries. Eq (5.8) is then solved in the interior ($0<Z<1$) and the value of $\psi^{(n)}$ is found along the upper and lower boundaries. Using (5.10) a new value of $\psi_Z^{(n)}$ along the boundaries at the next time step is found and the above process is repeated.

During the initial stages of the time integration, the values of $\psi^{(n)}$ are highly chaotic. As the integration proceeds, the unsteady eddy begins to move and grow at a more homogeneous rate, as dictated by the most unstable mode of the finite-difference set. Consequently, the time integration is terminated when the most unstable mode dominates all the other perturbations.

It is readily shown that the total kinetic plus potential energy behaves as $\exp(-2\lambda_i T)$. Therefore we may calculate $\lambda_i$ as $-\lambda_i = dE/dT/2E$ where, as it will be shown in Section 7,

$$E = \int_0^1 \int_0^{2\pi/\ell} \int_0^{2\pi} \frac{Ro\,\ell}{4\pi^2}\{\psi_X'^2 + \psi_Z'^2 + (1-\varepsilon Ro\psi_{X_0X_0}^{(E)})\psi_Y'^2\}dX_0 \; dY \; dZ \qquad (5.11)$$

In this manner we gain a contribution from each Fourier mode.

In determining $\lambda_r = \text{Re}(\lambda)$, we cannot use energy integrals such as

(5.11). However, using the Fourier component for n = 0 at the mid-level

(since it is the most accurately determined), we do find that

$$\lambda_r = \{\psi^{(0)*}(\tfrac{1}{2})\psi_T^{(0)}(\tfrac{1}{2})-\psi^{(0)}(\tfrac{1}{2})\psi_T^{(0)*}(\tfrac{1}{2})\}/2i|\psi^{(0)}(\tfrac{1}{2})|^2 \qquad (5.12)$$

Straightforward center differences in time and vertical space were used

throughout the investigation. The exception to this was the forward time

step taken initially. To damp the effects of the separation of the sol-

ution between the even- and odd-numbered time steps, which results from

a first-forward-then-centered time step, the first time step was sub-

divided into six subdivisions and time integration out to the first time

step was carried out using forward time steps.

Due to the coupling of the Fourier modes in (5.8), the system of linear

equations resulting from the finite-differencing of (5.8) gives a sparsely

populated matrix which must be inverted. Since this can be very time

consuming, we treat the right-hand side of (5.8) as a known quantity.

As a first quess we take $\psi^{(n)}$ as given from the previous time step (except

for the first time step when we set it equal to zero) and solve the tri-

diagonal system from the finite-differencing of the left-hand side of

(5.8). The $\psi^{(n)}$'s are then compared with the quessed values that were

used in the right-hand side. If they agree to within $10^{-5}$ (after all

the $\psi^{(n)}$'s have been properly normalized), then the calculation proceeds

to the calculation of the new $\psi_Z^{(n)}$ at Z = 0,1; otherwise, $\psi^{(n)}$ is used

as the new quess to evaluate the right-hand side of (5.8). This process

is repeated until convergence is obtained.

## 5.3. The approximate perturbation equations.

The solution of the perturbation equations using the numerical techniques described above is not entirely satisfactory. For small growth rates, we will be unable to find solutions to the perturbation equations since the background noise, which is produced when the random perturbations are introduced, completely masks the unstable mode. Also the errors associated with the finite differencing, especially for the higher harmonics, also limits the accuracy of the solution which are found.

For these reasons, we shall approximate the perturbation equations (5.8) by neglecting the right-hand side. Formally, such an approximation results in our neglecting $O(Ro^2)$ terms and we are, in fact, using the quasigeostrophic equations. However, as Hoskins (1975) has pointed out, there may be several occasions when the Jacobian terms in (3.34) may be neglected and yet the ageostrophic effects will be retained. Consequently, we shall apply the approximate perturbation equations to those situations where $Ro \ll 1$ as well as $Ro < 1$ and see how they compare to results obtained from the completely general equation (5.8).

Upon neglecting the terms on the right-hand side of (5.8), we may write the solution to $\Psi^{(n)}$ as

$$\psi' = \sum_{n=-\infty}^{\infty} \Psi^{(n)} \exp(i\{nkX_0 + \ell Y + \lambda T\}) \qquad (5.13)$$

where $\qquad \Psi^{(n)} = A_n \cosh m_n(Z-\tfrac{1}{2}) + B_n \sinh m_n(Z-\tfrac{1}{2})$

and $\qquad\qquad\qquad m_n = (n^2 k^2 + \ell^2)^{\frac{1}{2}}.$

Substituting (5.13) into the boundary conditions along $Z = 0,1$, the linear equations which form the eigenvalue problem for $\lambda$ are

$$(- i\varepsilon k\ell \ A \cosh(x) \ m_{n-1} \ \sinh(x_{n-1}) + i\varepsilon k^2\ell \ A \sinh(x) \ \cosh(x_{n-1}))A_{n-1}$$

$$+ (i\varepsilon k\ell \ A \cosh(x) \ m_{n+1} \ \sinh(x_{n+1}) - i\varepsilon k^2\ell \ A \sinh(x) \ \cosh(x_{n+1})) \ A_{n+1}$$

$$+ (-\varepsilon k\ell \ B \sinh(x) \ m_{n-1} \ \cosh(x_{n-1}) + \varepsilon k^2\ell \ B \cosh(x) \ \sinh(x_{n-1}))B_{n-1}$$

$$+ (-\varepsilon k\ell \ B \sinh(x) \ m_{n+1} \ \cosh(x_{n+1}) + \varepsilon k^2\ell \ B \cosh(x) \ \sinh(x_{n+1}))B_{n+1}$$

$$- 2\lambda \ m_n \ \sinh(x_n) \ A_n = 0 \qquad\qquad (5.14)$$

$$(- \varepsilon k\ell \ B \sinh(x) \ m_{n-1} \ \sinh(x_{n-1}) + \varepsilon k^2\ell \ B \cosh(x) \cdot \cosh(x_{n-1}))A_{n-1}$$

$$+ (- \varepsilon k\ell \ B \sinh(x) \ m_{n+1} \ \sinh(x_{n+1}) + \varepsilon k^2\ell \ B \cosh(x) \ \cosh(x_{n+1}))A_{n+1}$$

$$+ (-i\varepsilon k\ell \ A \cosh(x) \ m_{n-1} \ \cosh(x_{n-1}) + i\varepsilon k^2\ell \ A \sinh(x) \ \sinh(x_{n-1}))B_{n-1}$$

$$+ (+i\varepsilon k\ell \ A \cosh(x) \ m_{n+1} \ \cosh(x_{n+1}) - i\varepsilon k^2\ell \ A \sinh(x) \ \sinh(x_{n+1}))B_{n+1}$$

$$- 2\lambda \ m_n \ \cosh(x_n) \ B_n = 0 \qquad\qquad (5.15)$$

where $x = k/2$ and $x_n = m_n/2$. The coefficients of (5.14)-(5.15) are
sufficiently complicated and the matrices are sufficiently large
(for n = 0,1, there are six equations), so that (5.14) and (5.15)
were solved numerically.

Eqs (5.14)-(5.15) are solved along the lines outlined in Duffy (1975).
The infinite set of equations symbolized by (5.14)-(5.15) is truncated
by setting $A_n = B_n = 0$ for n $>$ N. This truncated set of equations is
solved and 4N+2 eigenvalues and eigenvectors are obtained. Upon taking
a larger N, in addition to new eigenvalues and eigenvectors corresponding
to the higher harmonics, eigenvalues and eigenvectors are found which
correspond to the eigenvalues and eigenvectors found in the system
with the smaller N but are of greater accuracy. Therefore, the process
of repeatedly expanding the system of truncated equations for larger and
larger N may be repeated until the desired accuracy is obtained.

The eigenvalues and eigenvectors were obtained by using a modified LR algorithm. In particular, a Fortran IV version of the Algol routines balance, comhes, comlr, comlr2, and balbak developed by Wilkinson et al (1971) were used. Balance and balbak were modified to handle the complex arrays.

## 5.4.  Check of the semigeostrophic equations.

As was shown in Section 3, the semigeostrophic equations are valid only under certain conditions which are given by (3.22)-(3.23). Before we can proceed to the numerical calculations, we must determine what values of $R_0$ and $\ell$ are allowed by the semigeostrophic equations for a given k.

Turning first to (3.22), we note that the largest term in the denominator will be $\bar{v}_g$;  the remaining terms will be of the order (or less) of the amplitude of the perturbations $u'_g$ and $v'_g$. In the numerator, the magnitude of the terms will be of the order of the perturbation's amplitude. Consequently, if k, $\ell$, and Ro are finite, the amplitude of the perturbations can always be so choosen so that (3.22) will be satisfied.

Turning to (3.23), we see that since $\bar{u}_g = 1$ the denominator will be of O(1). The numerator will, on the other hand, have terms of the order of the perturbation's amplitude. As in the case of (3.22), the perturbation's amplitude may always be so choosen so that (3.23) will be satisfied.

The mathematical problem now reduces to solving (5.8) and (5.10) or (5.14)-(5.15) for specific values of $\varepsilon$, $\ell$, and Ro. Before investigating this general problem, however, it is useful to consider some general stability criteria and energetics.

6. <u>Stability theorems</u>.

A great deal of useful information pertaining to our stability problem can be obtained by integral methods (see Charney and Stern, 1962). These theorems yield necessary conditions for instability and bounds on the growth and phase speeds of the disturbances.

6.1. Necessary conditions for instability.

Consider our meridional flow $v_g(X_0,Z)$ which is perturbed by a wave disturbance $\Psi(X_0,Z) \exp(i\ell Y+i\lambda T)$. We showed in the previous section that $\Psi(X_0,Z)$ satisfied (5.5) with the associated boundary conditions (5.6).

Suppose $\lambda \neq 0$, we multiply (5.5) by $\Psi^*$, integrate over a vertical cross section, and apply the boundary conditions (5.6). We obtain

$$\int_0^1 \int_0^{2\pi} |\Psi_Z|^2 + |\Psi_{X_0}|^2 + \ell^2 (1-\varepsilon Ro\psi^{(E)}_{X_0 X_0}) |\Psi|^2 \, dX_0 dZ = \int_0^{2\pi} \frac{\varepsilon\psi^{(E)}_{X_0 Z}\ell |\Psi|^2}{(\varepsilon\ell \psi^{(E)}_{X_0}+\lambda)^2}\Bigg|_{Z=0}^{Z=1} dX_0 \quad (6.1)$$

The real and imaginary parts of this integral must be satisfied separately.

The imaginary part yields $\lambda_i \int_0^{2\pi} \frac{\varepsilon\ell\psi^{(E)}_{X_0 Z} |\Psi|^2}{|\varepsilon\ell\psi^{(E)}_{X_0} + \lambda|^2}\Bigg|_{Z=0}^{Z=1} dX_0 = 0 \quad (6.2)$

If $\lambda_i$ is not to equal zero, then it is necessary that the integral quantity vanish. The vanishing of this integral is thus a necessary condition for instability. If unstable perturbations exist their instability is a result of the boundary variations of the potential temperature of the basic state. Consequently any instabilities which are found arise from the baroclinic, rather than the barotropic, nature of the basic state.

More information can be obtained from the real part of (6.1)

$$\int_0^1 \int_0^{2\pi} |\Psi_Z|^2 + |\Psi_{X_0}|^2 + \ell^2(1-\epsilon Ro \,\psi^{(E)}_{X_0 X_0}) \, |\Psi|^2 \, dX_0 \, dZ =$$

$$\ell^2 \int_0^{2\pi} \frac{\epsilon^2 \psi^{(E)}_{X_0} \psi^{(E)}_{X_0 Z} |\Psi|^2}{|\epsilon \ell \psi^{(E)}_{X_0} + \lambda|^2} \Bigg|_{Z=0}^{Z=1} dX_0 \; + \; \ell\lambda_r \int_0^{2\pi} \frac{\epsilon \psi^{(E)}_{X_0 Z} |\Psi|^2}{|\epsilon\ell\psi^{(E)}_{X_0}+\lambda|^2} \Bigg|_{Z=0}^{Z=1} dX_0 \quad (6.3)$$

For unstable waves, the third term which is multiplied by $\lambda_r$ must vanish according to (6.2). In addition, $(1-\epsilon Ro\psi^{(E)}_{X_0 X_0})$ is always greater than zero for the vertical component of the absolute vorticity to remain finite. Thus a necessary condition for instability is

$$\int_0^{2\pi} \frac{\psi^{(E)}_{X_0} \psi^{(E)}_{X_0 Z} |\Psi|^2}{|\epsilon\ell\psi^{(E)}_{X_0} + \lambda|^2} \Bigg|_{Z=0}^{Z=1} \; > \; 0.$$

Hence a sufficient condition for <u>stability</u> is that

$$\psi^{(E)}_{X_0}(X_0,1)\psi^{(E)}_{X_0 Z}(X_0,1) \; < \; 0$$

and

$$\psi^{(E)}_{X_0}(X_0,0)\psi^{(E)}_{X_0 Z}(X_0,0) \; > \; 0 \qquad \text{everywhere.}$$

## 6.2. Phase speed and growth rate.

In this subsection, we shall derive certain bounds for the speed of propagation and growth rates of unstable waves.

Since $\lambda_i$ is not zero, we may make the transformation: $\Psi = (\epsilon\ell\psi^{(E)}_{X_0} - \lambda)\chi$.

Upon making the substitution into (5.5)-(5.6) and simplifying, we find

$$\{(\epsilon\ell\psi_{X_0}^{(E)}-\lambda)^2 \chi_Z\}_Z + \{(\epsilon\ell\psi_{X_0}^{(E)}-\lambda)^2 \chi_{X_0}\}_{X_0} - \ell^2(1-\epsilon\,Ro\psi_{X_0 X_0}^{(E)})(\epsilon\ell\psi_{X_0}^{(E)}-\lambda)^2 \chi = 0 \tag{6.5}$$

$$\chi_Z = 0 \tag{6.6}$$

along $Z = 0,1$. Multiplying (6.5) by $\chi^*$, and integrating over a zonal cross section, and applying (6.6), we obtain

$$\int_0^1 \int_0^{2\pi} (\epsilon\ell\psi_{X_0}^{(E)}-\lambda)^2 \{|\chi_Z|^2 + |\chi_{X_0}|^2 + \ell^2(1-\epsilon\,Ro\psi_{X_0 X_0}^{(E)})|\chi|^2\}\ dX_0\ dZ = 0 \tag{6.7}$$

Taking the imaginary part of (6.7), we find

$$\int_0^1 \int_0^{2\pi} (\epsilon\ell\psi_{X_0}^{(E)}-\lambda_r)\{|\chi_Z|^2 + |\chi_{X_0}|^2 + \ell^2(1-\epsilon\,Ro\psi_{X_0 X_0}^{(E)})|\chi|^2\}\ dX_0\ dZ = 0 \tag{6.8}$$

It is clear from (6.8) that $\lambda_r/\epsilon\ell$ cannot be greater than the maximum velocity nor less than the minimum velocity of the meridional flow. Further, there must exist a line in the $X_0$-$Z$ plane on which the phase speed of the unstable wave (i.e., $\lambda_r/\ell$) is equal to the local fluid velocity.

If we define

$$|\chi_Z|^2 + |\chi_{X_0}|^2 + \ell^2(1-\epsilon\,Ro\psi_{X_0 X_0}^{(E)})|\chi|^2 \equiv Q$$

and

$$\int_0^1 \int_0^{2\pi} (\ )\ dX_0\ dZ = \overline{(\ )},$$

then the real part of (6.7) may be written as

$$\overline{\epsilon^2\ell^2\psi_{X_0}^{(E)2}Q} - \overline{2\ell\lambda_r\psi_{X_0}^{(E)}Q} + (\lambda_r^2-\lambda_i^2)\overline{Q} = 0 \tag{6.9}$$

and the imaginary part as

$$\overline{\epsilon\ell\psi_{X_0}^{(E)}Q} - \lambda_r\overline{Q} = 0. \tag{6.10}$$

Applying (6.10) to (6.9)

$$\varepsilon^2 \ell^2 \overline{\psi_{X_0}^{(E)2} Q} = (\lambda_r^2 + \lambda_i^2) \overline{Q}. \tag{6.11}$$

Since we can always choose a $V_{max}$ and $V_{min}$ such that

$$0 \geq \varepsilon^2 \ell^2 \overline{(\psi_{X_0}^{(E)} - V_{max})(\psi_{X_0}^{(E)} - V_{min})Q}$$

$$0 \geq \varepsilon^2 \ell^2 \overline{(\psi_{X_0}^{(E)2}Q)} - (V_{max}+V_{min})\varepsilon^2 \ell^2 \overline{\psi_{X_0}^{(E)} Q} + \varepsilon^2 \ell^2 V_{max}V_{min}\overline{Q}, \tag{6.12}$$

we can form the inequality

$$0 \geq (\lambda_r - \tfrac{1}{2}\varepsilon\ell (V_{max}+V_{min}))^2\overline{Q} + \lambda_i^2 \overline{Q} - (\tfrac{1}{2}\varepsilon\ell (V_{max}-V_{min}))^2\overline{Q} \tag{6.13}$$

or $\qquad (\tfrac{1}{2}\varepsilon\ell (V_{max}-V_{min}))^2 \geq (\lambda_r - \tfrac{1}{2} \varepsilon\ell(V_{max}+V_{min}))^2 + \lambda_i^2 \tag{6.14}$

According to (6.14), $\lambda$ lies, for unstable waves, in a semicircle whose

radius is given by the square root of the left-hand side of (6.14) while

the origin of the semicircle is on the real axis of the $\lambda$ plane at the

mean velocity of the meridional flow.

To obtain an upper bound on $\lambda_i$, we use (6.14) to obtain

$$\lambda_i^2 \leq \tfrac{1}{4}\varepsilon^2 \ell^2 (V_{max}-V_{min})^2 \tag{6.15}$$

As we would expect, when the velocity field becomes uniform (i.e., $V_{max} = V_{min}$), the growth rate vanishes. It should also be noted that the upper

bound on $\lambda_i$ does not depend upon the Rossby number. For our particular

flow, $V_{max} = - V_{min} = 3.07$.

## 7. Energetics.

In order to clarify the nature of the instabilities found in the next section, we shall derive in this section energy equations for both the exact and the approximate perturbation equations. We will then be able to describe the conversion of available potential energy (APE) into kinetic energy and _vice versa_ between the baroclinic wave and the perturbations.

### 7.1. The exact energy equation.

The energy equation for the constant potential vorticity model can be derived from (3.38) and (5.2). We may write these equations in the form:

$$\left(\frac{\partial}{\partial T} + \varepsilon\psi_{X_0}^{(E)}\frac{\partial}{\partial Y}\right)\left(\psi'_{ZZ} + \psi'_{X_0 X_0} + (1-\varepsilon Ro\psi_{X_0 X_0}^{(E)})\psi'_{YY}\right) = 0 \qquad (7.1)$$

and

$$\left(\frac{\partial}{\partial T} + \varepsilon\psi_{X_0}^{(E)}\frac{\partial}{\partial Y}\right)\psi'_Z - \varepsilon\psi_{X_0 Z}^{(E)}\psi'_Y + (Ro^{-1} + \varepsilon\psi_{ZZ}^{(E)})w' = 0 \qquad (7.2)$$

Taking the Z derivative of (7.2), (7.1) can be rewritten

$$\left(\frac{\partial}{\partial T} + \varepsilon\psi_{X_0}^{(E)}\frac{\partial}{\partial Y}\right)\{\psi'_{X_0 X_0} + \psi'_{YY}(1-\varepsilon Ro\psi_{X_0 X_0}^{(E)})\} + \varepsilon\psi_{X_0 ZZ}^{(E)}\psi'_Y - Ro^{-1}w' - (w\varepsilon\psi_{ZZ}^{(E)})_Z = 0$$
$$(7.3)$$

Turning our attention first to the thermodynamics equation, we multiply it by $\psi'_Z$ and integrate over the volume:

$$\frac{\partial}{\partial T}\iiint_V \tfrac{1}{2}Ro\,\psi'^2_Z\,dV = \iiint_V \varepsilon Ro\,\psi_{X_0 Z}^{(E)}\psi'_Z\psi'_Y - (1-\varepsilon Ro\psi_{X_0 X_0}^{(E)})\,w'\psi'_Z\,dV \qquad (7.4)$$

where

$$\iiint_V (\ )\,dV = \frac{1}{2\pi}\int_0^{2\pi}\frac{\ell}{2\pi}\int_0^{2\pi/\ell}\int_0^1 (\ )\,dZ\,dY\,dX_0.$$

The left-hand side of (7.4) represents the rate of change of the pertur-

bation's APE. The right-hand side of (7.4) reveals that the perturbation's

APE is generated by the baroclinic instability of the finite-amplitude

baroclinic wave, and depleted by the conversion of the perturbation's APE

to its kinetic energy by the rising of warm air and the sinking of cold

air.

It should be noted that the second term on the right-hand side of (7.4)

contains the term $(1+\varepsilon Ro\psi_{ZZ}^{(E)})$. This corresponds to a modification of the

static stability of the mean atmosphere due to the presence of the baro-

clinic wave.

Turning our attention now to the perturbation kinetic energy, we mul-

tiply (7.3) by $\psi'$ and integrate over the volume to obtain

$$\frac{\partial}{\partial T} \iiint_V \tfrac{1}{2}Ro\{\psi_{X_0}'^2 + (1-\varepsilon Ro\psi_{X_0 X_0}^{(E)})\psi_Y'^2\}dV = \iiint_V (1-\varepsilon Ro\psi_{X_0 X_0}^{(E)})w'\psi_Z' + \varepsilon Ro\psi_{X_0 X_0}^{(E)}\psi_{X_0}'\psi_Y' \, dV.$$

$$(7.5)$$

The terms on the left-hand side of (7.5) represent the rate of growth

of the perturbation kinetic energy. It should be noted that the

$(1 - \varepsilon Ro\ \psi_{X_0 X_0}^{(E)})$ term which multiplies $\psi_Y'^2$ results from the distortion

introduced by the Eliassen coordinates.

The generation of the perturbation kinetic energy is due to two effects.

The first term on the right-hand side of (7.5) represents the conversion

of perturbation APE into perturbation kinetic energy through warm air

rising and cold air sinking. The second term represents a barotropic in-

stability from the horizontal shear generated by the finite-amplitude baro-

clinic wave which feeds its kinetic energy into the perturbations through

the Reynolds stresses $\psi_{X_0}'\psi_Y'$.

Consequently the total energy equation may be written as

$$\frac{\partial}{\partial T} \iiint\limits_{V} \tfrac{1}{2}Ro\{\psi_Z'^2 + \psi_{X_0}'^2 + (1-\varepsilon Ro\psi_{X_0X_0}^{(E)})\psi_Y'^2\}dV =$$

$$= \iiint\limits_{V} \varepsilon Ro\ \psi_{X_0Z}^{(E)}\ \psi_Z'\psi_Y' + \varepsilon Ro\psi_{X_0X_0X_0}^{(E)}\ \psi_X'\ \psi_Y'\ dV \qquad (7.6)$$

## 7.2. The approximate energy equation.

We may derive the approximate energy equation by neglecting the

$$-\left[\frac{\partial}{\partial T} + \varepsilon\psi_{X_0}^{(E)}\frac{\partial}{\partial Y}\right]\varepsilon Ro\psi_{X_0X_0}^{(E)}\psi'_{YY}$$ term in (7.3). The derivation then pro-

ceeds as before and we obtain (7.4),

$$\frac{\partial}{\partial T}\iiint\limits_{V} \tfrac{1}{2}Ro\{\psi_{X_0}'^2 + \psi_Y'^2\}\ dV = \iiint\limits_{V}(1-\varepsilon Ro\psi_{X_0X_0}^{(E)})\ w'\psi_Z' + \varepsilon Ro\psi_{X_0X_0}^{(E)}\ \psi_X'\ \psi_Y'\ dV \qquad (7.7)$$

and

$$\frac{\partial}{\partial T}\iiint\limits_{V}\tfrac{1}{2}Ro\{\psi_Z'^2 + \psi_{X_0}'^2 + \psi_Y'^2\}dV = \iiint\limits_{V}\varepsilon Ro\psi_{X_0Z}^{(E)}\ \psi_Z'\psi_Y' + \varepsilon Ro\psi_{X_0X_0}^{(E)}\ \psi_X'\ \psi_Y'\ dV \qquad (7.8)$$

The interpretations of the source terms can be made in the same manner as above.

An important point concerning our set of approximate energy equations is that, despite our neglecting certain terms in the exact perturbation equations, we have done it in such a manner that we have not generated fictious sources of energy. Rather we have only modified the definition of the perturbation kinetic energy. This suggests that our choice of approximate perturbation equations is physically realistic.

We may summarize the energetics, irrespective of whether we are using the exact or approximate perturbation equations, as shown in Fig 3.
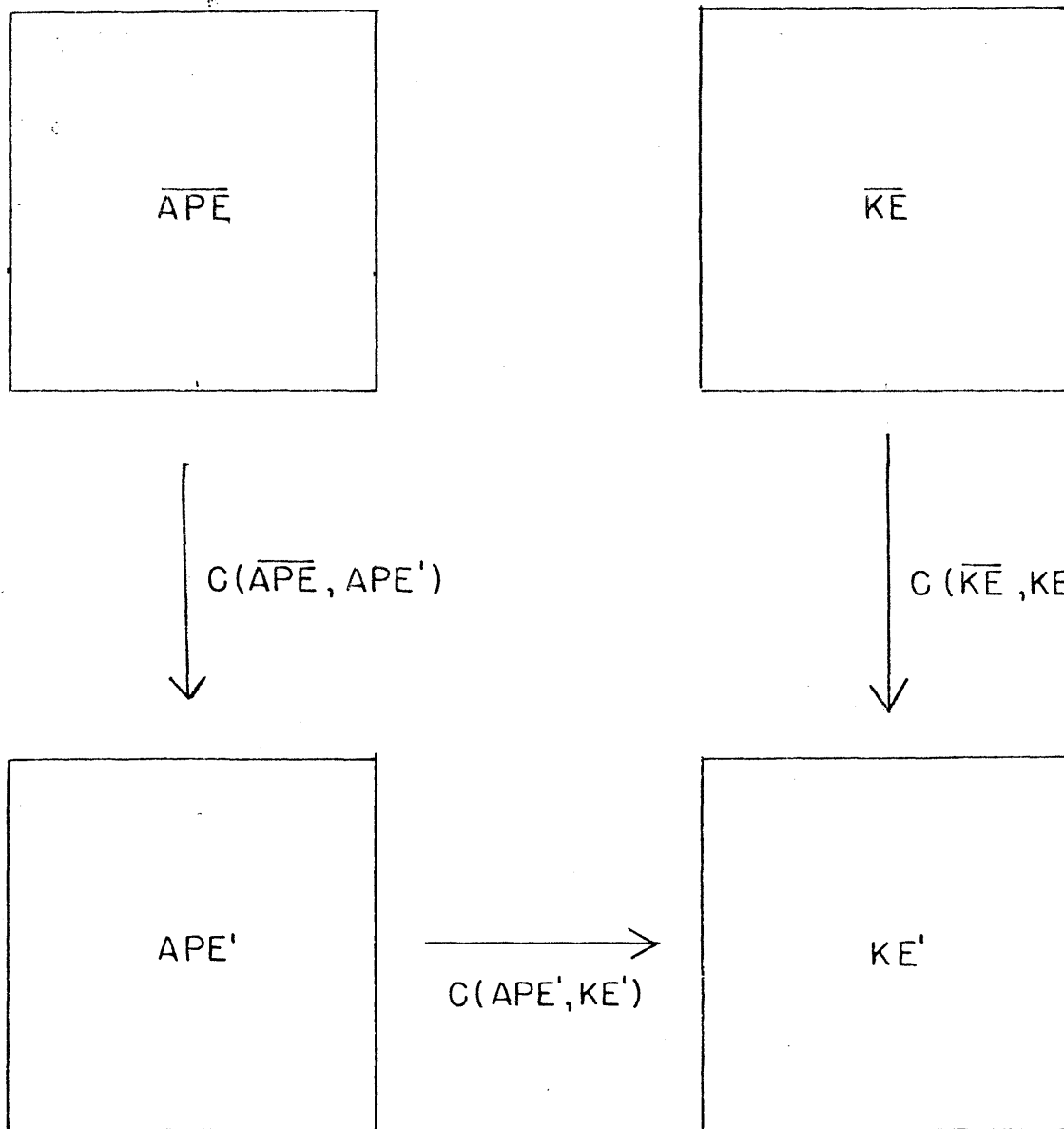
Fig 3.  Energy flow diagram for the constant potential vorticity model.

## 8. Results.

Eigenvalue solutions to (5.8) and (5.10) as well as (5.14)-(5.15) were

obtained for $\epsilon k Ro = 0.1$ and $0.4$ for $\ell$ varying from $0.1$ to $2.0$.

### 8.1. The approximate perturbation equations.

In the solutions to the approximate perturbation equations, eigenvalues

of the form $\pm|\lambda_r| \pm i|\lambda_i|$ were always found. These eigenvalues would

further be classified according to whether $|\lambda_r| = 0$, $|\lambda_i| = 0$, or

neither. (For convenience, $\lambda = 0$ has been incorporated into the $|\lambda_r| = 0$

class.) Since the approximate perturbation equations are independent of

Ro, all the $|\lambda_r|$'s and $|\lambda_i|$'s which were found could be displayed on

$|\lambda_r/\epsilon\ell|$ -$\ell$ and $|\lambda_i/\epsilon|$ -$\ell$ planes. However, since we are interested in

the most unstable solutions, we shall restrict ourselves to the three

largest $|\lambda_i|$'s.

In Fig 4 we depict the variations of $|\lambda_r/\epsilon\ell|$ with $\ell$ for the three most

unstable modes. In Fig 5, we give the corresponding $|\lambda_i/\epsilon|$ for each of

the curves presented in Fig 4.

Curve A in Figs 4 and 5 illustrates the behavior of the unstable,

stationary perturbation (i.e., $|\lambda_r| = 0$) found in the calculations. As

shown in Fig 4, these unstable stationary perturbations existed only

for $\ell$'s below a critical value, approximately 1.6. For $\ell$'s greater

than this critical $\ell$, the stationary perturbation ended and a non-

stationary perturbation was generated.

It was found that the stationary perturbations, when they existed,

were the most unstable. The magnitude of $|\lambda_i/\epsilon|$ increased as $\ell$ increased

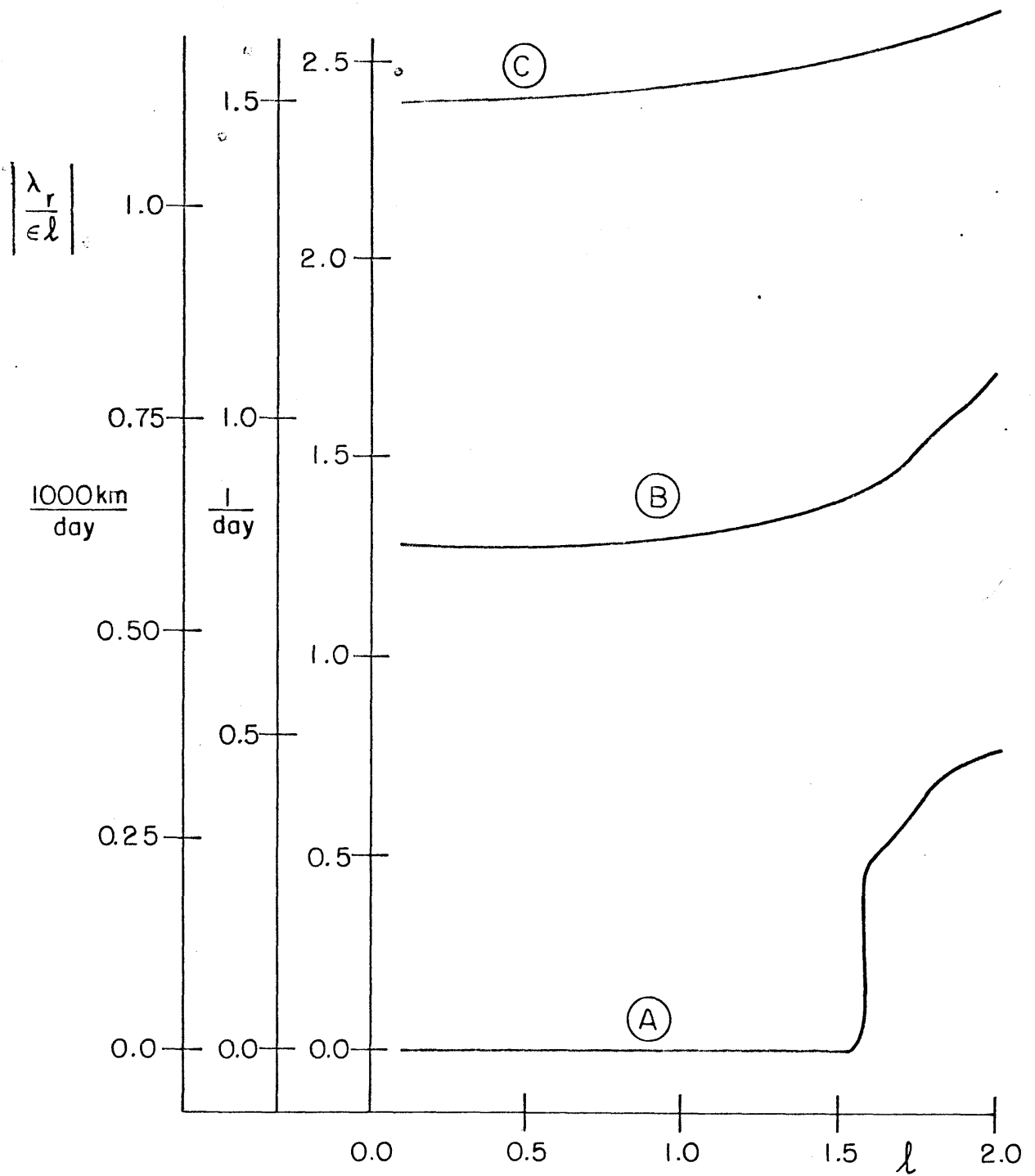from 0.1 to 1.0 and then decreased as $\ell$ increased as 1.6. In the region

Fig 4. Absolute magnitude of the real part of $\lambda/\varepsilon\ell$ as a function of $\ell$

for the three most unstable modes (right-most scale). The center

and left scales give this phase speed in units of $d^{-1}$ for Ro = 0.187
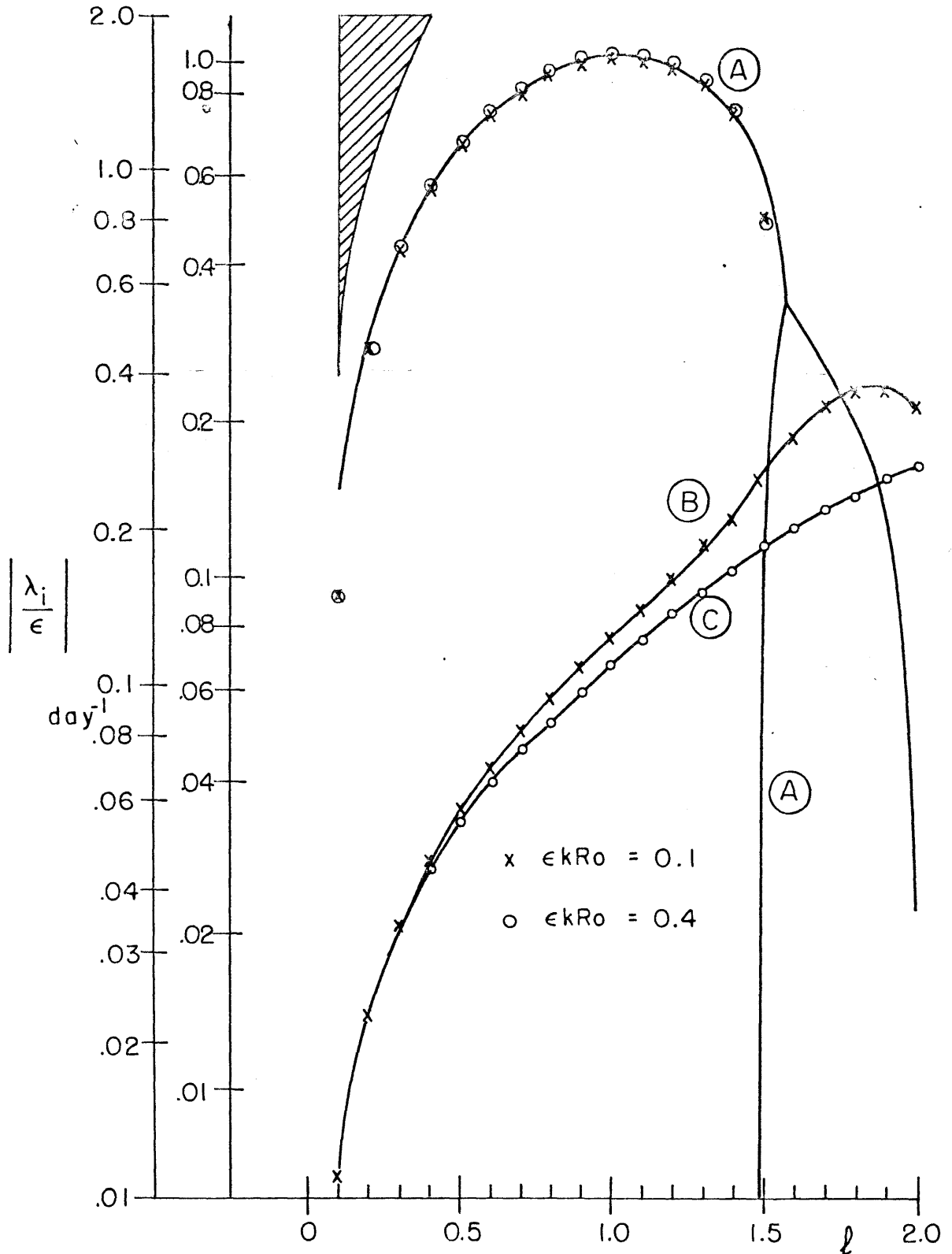
and $10^3$ km/d if L $\doteq$ 750 km.

Fig 5. The absolute value of the imaginary part of $\lambda/\varepsilon$ as a function of $\ell$ for the three most unstable modes (right-most scale) from both the exact and approximate perturbation equations. The dimensional growth rate given by the left-most scale for Ro = 0.187. The shaded area indicates those eigenvalues which are forbidden by stability theorem (6.15).

of $\ell = 1.5$, a $\lambda = 0$ solution developed a nonzero $|\lambda_i|$ whose magnitude increased extremely rapidly as $\ell$ increased. This stationary perturbation then joined the other stationary perturbation approximately at $\ell = 1.55$. After this point of junction, a nonzero $|\lambda_r|$ developed; as $\ell$ increased further, $|\lambda_r/\epsilon\ell|$ increased and $|\lambda_i/\epsilon|$ decreased. Although not shown in Fig 5, these nonstationary perturbations eventually became neutrally stable.

Of the eigenvalues found, the majority fell into the classification of nonzero $|\lambda_r|$ and $|\lambda_i|$. Curves B and C in Figs 4 and 5 are typical of those found in this classification and were choosen for presentation since they possessed the largest growth rates of the nonstationary perturbations found. It was further found that for $\ell \ll 1$ there was associated with each $\pm |\lambda_r| \pm i |\lambda_i|$, another $\pm|\lambda_r'| \pm i |\lambda_i'|$ such that $|\lambda_r| \simeq |\lambda_r'|$ and $| \lambda_i| \simeq |\lambda_i'|$ with $|\lambda_r| > |\lambda_r'|$ and $|\lambda_i| > |\lambda_i'|$. As $\ell$ increased the magnitude of $|\lambda_i'|$ decreased and eventually this eigenvalue became neutrally stable. The $|\lambda_i|$'s, on the other hand, grew as $\ell$ increased and then, at a critical point, started to decrease towards zero. Eventually, these unstable perturbations also became neutrally stable.

## 8.2 The exact perturbation equations.

Eqs (5.8) and (5.10) were solved numerically to obtain $\lambda$ as described in Section 5. There were 41 points in the vertical and (5.2) was truncated so that the Fourier components ran from n = -10 to +10. On Fig 5 we have plotted "data points" obtained from our numerical experiment for various $\epsilon k Ro$. As can be readily seen, the agreement between the $|\lambda_i/\epsilon|$'s found using the approximate and exact perturbation equations is excellant

for $\ell \leq 1.5$. This is also true for $|\lambda_r/\varepsilon\ell|$ which was found to be very

close to zero. Beyound $\ell = 1.5$, solutions could not be obtained due

to the smallness of the growth rates that may have been present and the

noise which was introduced during initialization. Consequently we

cannot absolutely confirm the existence of the nonstationary perturbations

found above using the approximate perturbation equations.

When (5.8) was finite-differenced in the vertical, inhomogenous terms

were generated in two different ways. The first was from the evaluation

of the terms on the right-hand side of (5.8) with the quessed values of

$\psi^{(n)}$; the second was the use of the boundary conditions, i.e., $\psi_Z^{(n)}$

specified along $Z = 0,1$, to eliminate $\psi^{(n)}(0)$ and $\psi^{(n)}(1)$ from the

system of linear equations. Upon comparing these two effects, it was

found that the boundary effects greatly dominated over the terms gen-

erated by the right-hand side of (5.8). Consequently, the solutions to

(5.8) were determined mostly by the boundary effects. This is reflected

in the very good agreement between the results obtained from the

approximate and exact perturbation equations since the approximate

perturbation equations merely neglect the terms on the right-hand side

of (5.8).


8.3.  Energetics.

In Table 1, the energetic conversions are listed which took place for

the most unstable perturbation. Since the results from the exact per-

turbation equations are essentially independent of Ro, we have given the

energetics for the case when $\varepsilon k Ro = 0.3$. We have also normalized all the

conversions by taking $C(\overline{APE},APE')$ to equal 1. It was found that the

Table 1. Normalized energy conversion rates for the most unstable perturbation ( $\ell$ = 1.0 ) found in the constant potential vorticity model.

| Conversion | Exact perturbation equations for $\epsilon kRo$ = 0.3 | Approximate perturbation equations |
|---|---|---|
| C(APE,APE') | 1.00000 | 1.00000 |
| C(APE',KE') | 0.16417 | 0.16460 |
| C($\overline{KE}$,KE') | 0.39248 | 0.35680 |

perturbation received energy not only from the APE of the baroclinic wave but also the KE. Some of the perturbation's APE was then transformed into the perturbation's KE.

Further computations revealed that when $|\lambda_r| \neq 0$, in the approximate perturbation solutions, the perturbation received APE from the baroclinic wave and some of the perturbations's APE was then transformed into the perturbation's KE. However, unlike the $|\lambda_r| = 0$ case, some of the solutions were found to transform the perturbation's KE into the KE of the baroclinic wave.


8.4.  Physical interpretation of the results.

As Fig 5 shows, the most unstable perturbations are associated with $\ell = 1$. Furthermore, upon examining the eigenvectors, it is found that the Fourier coefficients having the largest amplitude have n = 0, ±1; the amplitude of the n = ±2 Fourier components are approximately 10% of the amplitude for n = ±1. Consequently, the length scale of the most unstable perturbation in both the zonal and meridional directions is the Rossby radius of deformation.

In our model there are two possible sources of instability:  conventional baroclinic instability and Rayleigh instability. Since our basic state never generates the small Richardson numbers necessary for either Kelvin-Helmholtz or "symmetric" instabilities (similar to those found by Gambo and Tokioka, see pg. 13) to become important, we need not consider these types of instability further.

Unquestionably the instabilities found in the previous sections result in part from conventional baroclinic instability.  In the previous

sections, we have shown that the instabilities found in this thesis

(1) arise from variations of the basic state's potential temperature

along the horizontal boundaries, (2) grow by conversion of the basic

state's available potential energy into the perturbation's available

potential energy, and (3) have a characteristic length scale of the

order of the Rossby radius of deformation - all properties which are

characteristic of conventional baroclinic instability.

In our model, we have taken the potential vorticity of our basis

state to be constant and the potential vorticity of the perturbations

to be zero. In the case of quasigeostrophic flow, Charney and Stern

(1962) have shown that there are two possible sources of instability

in a baroclinic-barotropic circumpolar vortex. One of the sources

of instability is the variations of the potential temperature along

the horizontal boundaries. We have this type of instability in our

model and it is associated with conventional baroclinic instability.

Another source of instability is due to the vanishing of the meridional

derivative of the potential vorticity in an isoentropic surface or the

pseudopotential vorticity in a level surface somewhere within the flow.

In our problem, this would correspond to a vanishing of the meridional

derivative of the basis state's potential vorticity somewhere within

the flow. This does not occur in our problem and has the consequence

of excluding Rayleigh instability in the flow.

Another intriguing aspect of our perturbation analysis is that the

results are mathematically isomorphic to those for a finite-amplitude

Rossby wave in a perturbation analysis employing the quasigeostrophic

equations. In the previous sections, we have shown that a baroclinic

wave with a strong frontal zone which is described by the semigeostrophic equations in Eliassen coordinates is mathematically, though not physically, isomorphic to an Eady wave without a frontal zone.

In summary, Hoskins and Bretherton's constant potential vorticity model for describing frontogenesis as a large-scale, finite-amplitude wave in a zonal flow leads to frontal instabilities which themselves are essentially of baroclinic character, not shear instabilities of the Rayleigh type. For the latter to exist, gradients of potential vorticity in the basic state flow are required.

9. Kinematics of the unstable wave.

In this section we shall display the pressure, temperature, velocity, and vorticity fields associated with the most unstable perturbation found in the previous section. For concreteness, we shall take $\varepsilon = 1$, $Ro = 0.187$, $k = 1.60$. With these values, the most unstable perturbation is a stationary perturbation with $kc_i$ of 1.7 $d^{-1}$, corresponding to a doubling time of 10 hr, and $\ell = 1.00$. Since the amplitude of the perturbation is arbitary, we shall take it to be 10% of the basic state's amplitude (except for w and the relative vorticity which have been normalized so that most of the values plotted are $O(1)$).

Figure 6 shows the total pressure field (perturbation plus basic state) at $z = 1/2$. The pressure perturbation is such that intensification of the basic state trough occurs between $y = \pi/2$ and $3\pi/2$ and pressure rises occur between $y = 0$ and $\pi/2$ and $3\pi/2$ and $2\pi$. Since the perturbation pressure field is slightly out of phase with the basic state trough (in the x direction) there is a slight asymmetry in the total pressure field.

Figure 7 shows the total potential temperature field at the level $z = 1/2$. From this figure we see that there are intrusions of cold and warm air across the frontal surface (located at $kx = \pi$ at $z = 1/2$). These intrusions of warm and cold air are characteristic of the baroclinic instability of our model where there is a positive correlation between $u'$ and $\theta'$.

Figure 8 shows the total potential temperature field at $z = 0$. As would be expected of a baroclinic instability, relatively colder air predominates in the lower levels. It should be note that

the only large area of warm air left is in the lower right quadrant.  We

shall return to this point in the next section.

Figure 9 presents the vertical velocity field at $z = 1/2$.  As would

expected, the largest vertical velocities are in the neighborhood of the

frontal surface where warm air is rising and cold air is sinking.  We

shall also return to this figure in the next section.

Figures 10-13 show vertical cross sections of the total potential

temperature and total velocity fields.  As would be expected of a

baroclinic instability, there is rising motion associated with warm

air and sinking motion with cold air.  The u velocity field (with the

constant $\bar{u} = 1$ subtracted out) shows that sinking cold air would spread

out in the lower levels while the rising warm air will expand in the

upper regions.

Figure 14 shows the relative vorticity field associated with the

perturbations.  From the figure we see that the largest cyclonic

as well as anticyclonic vorticity occur in the neighborhood where

the frontal surface intersects the plates.  Intense centers of

cyclonic and anticyclonic vorticity are in qualitative agreement

with the atmospheric observations of frontal cyclones as noted by

Palmen and Newton (1969, Section 10.9).
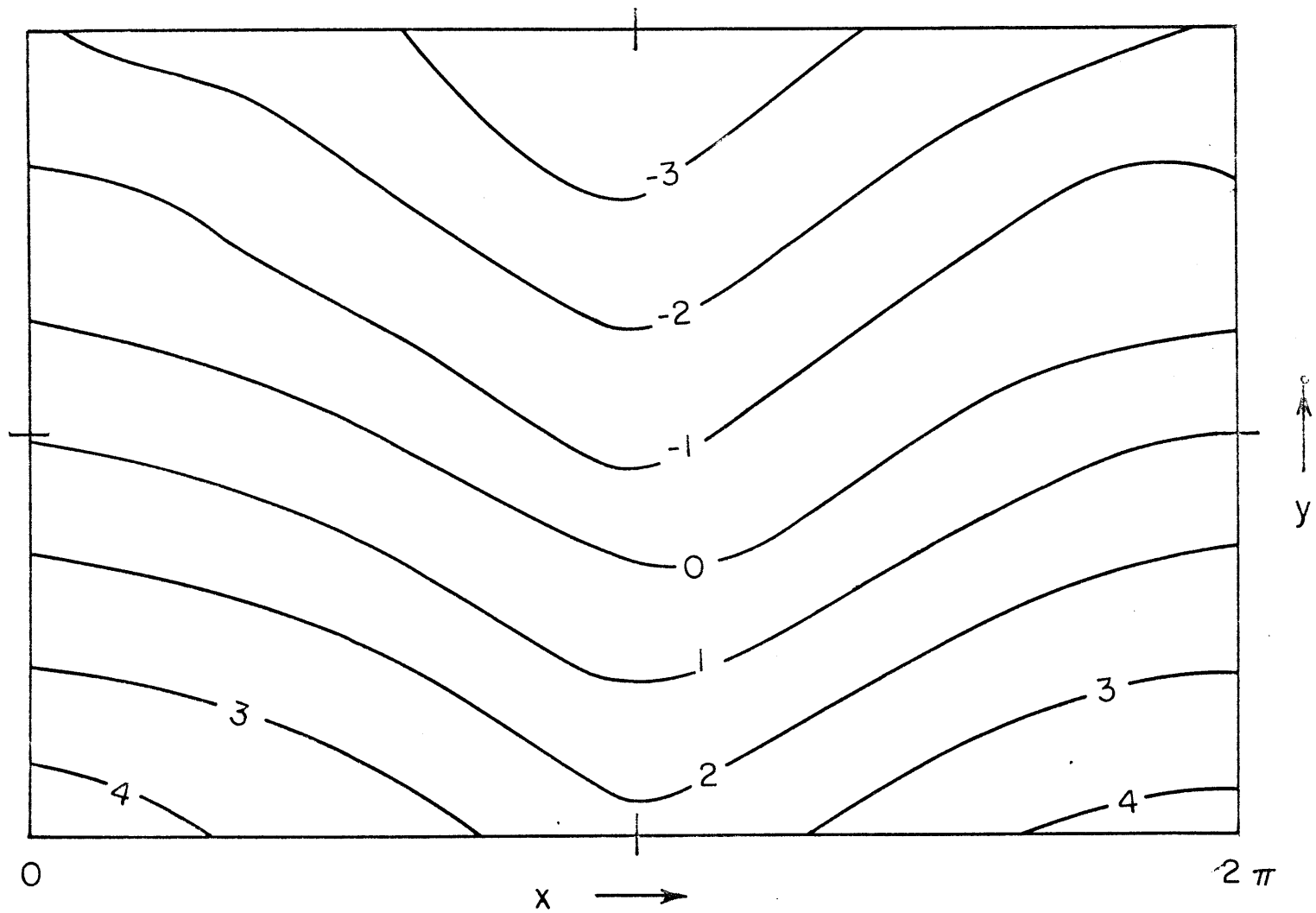
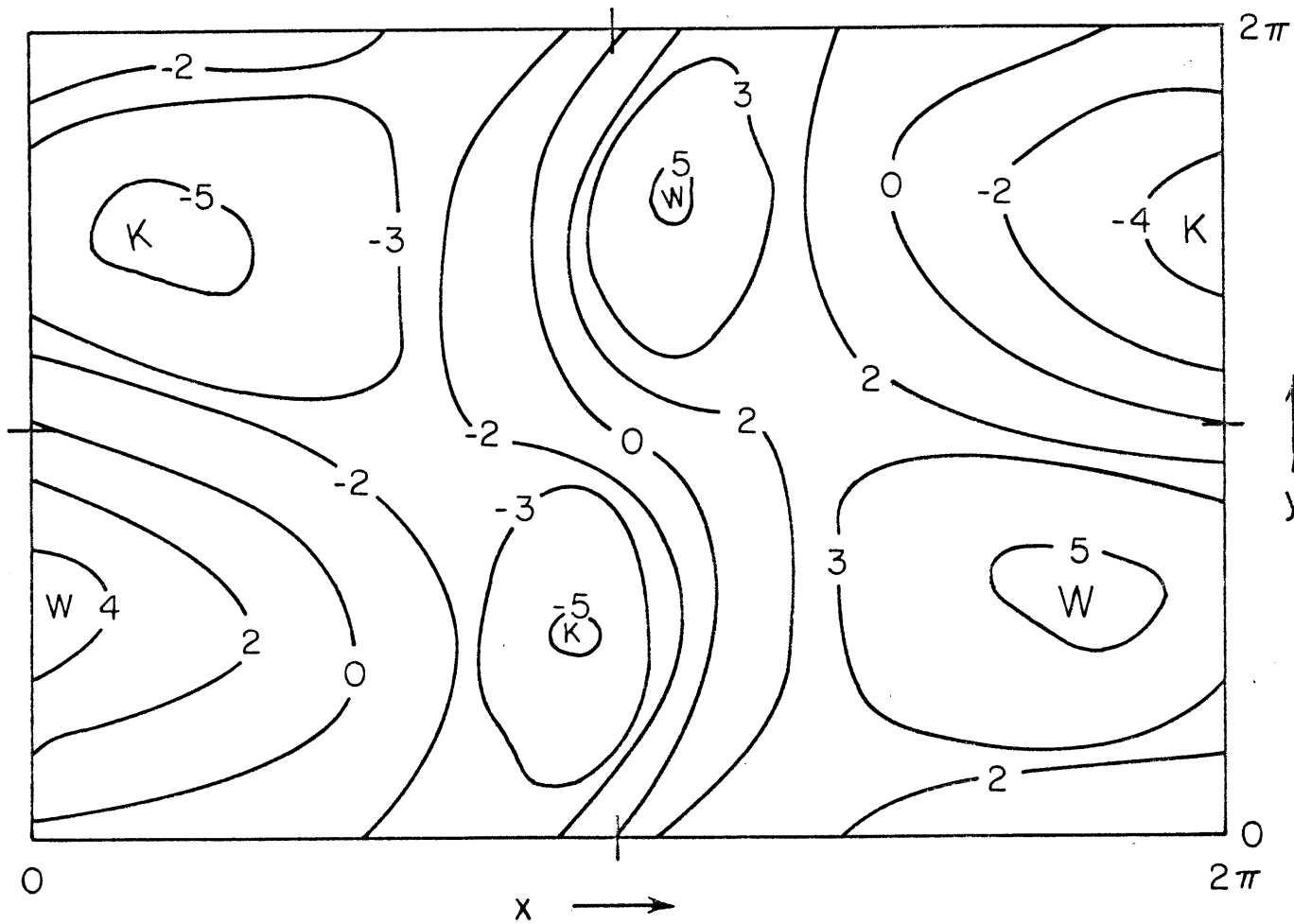Fig 6.   Total pressure field at z = 1/2 in nondimensional units.

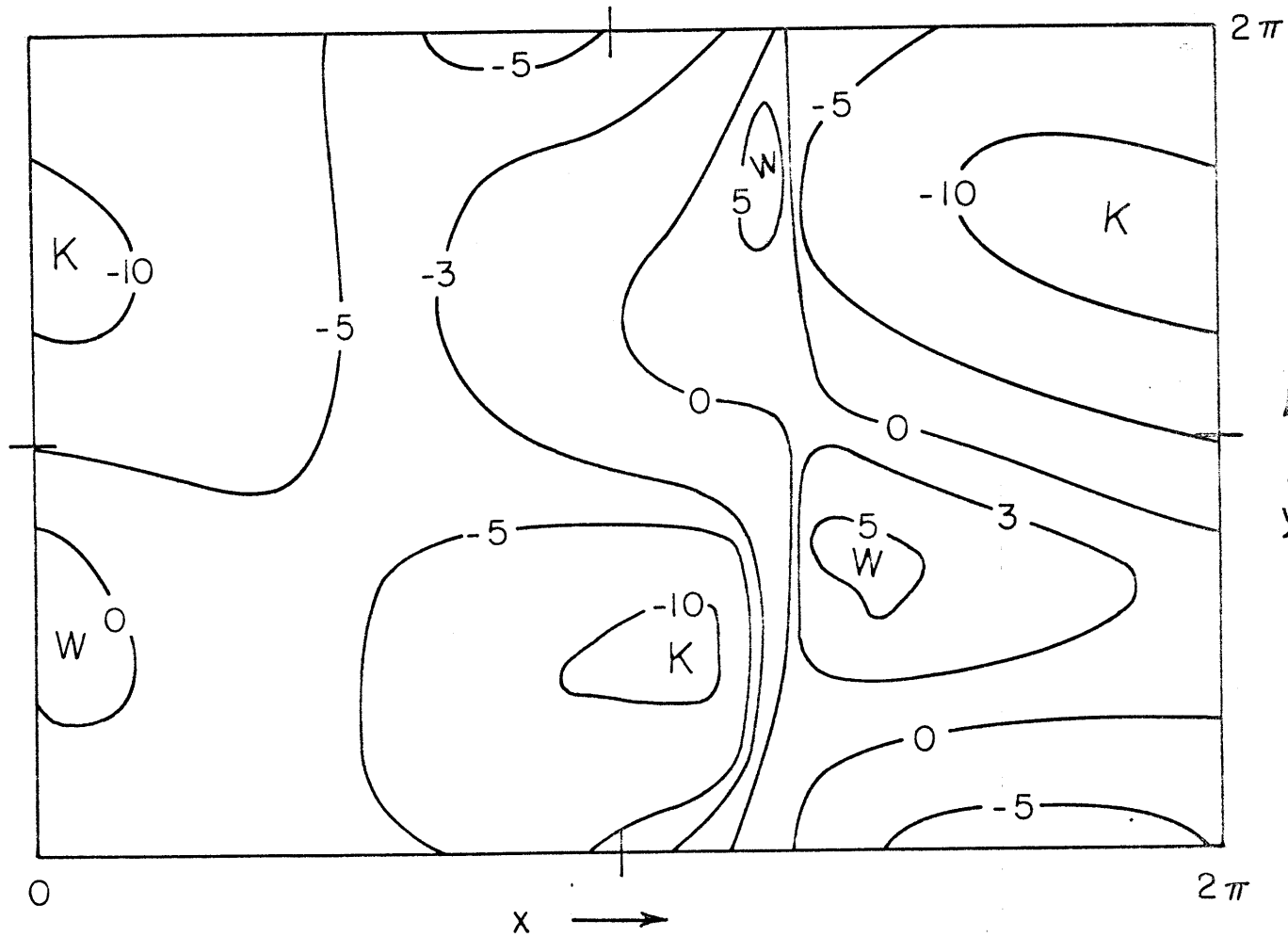Fig 7. Total potential temperature field at z = 1/2 in nondimensional units.

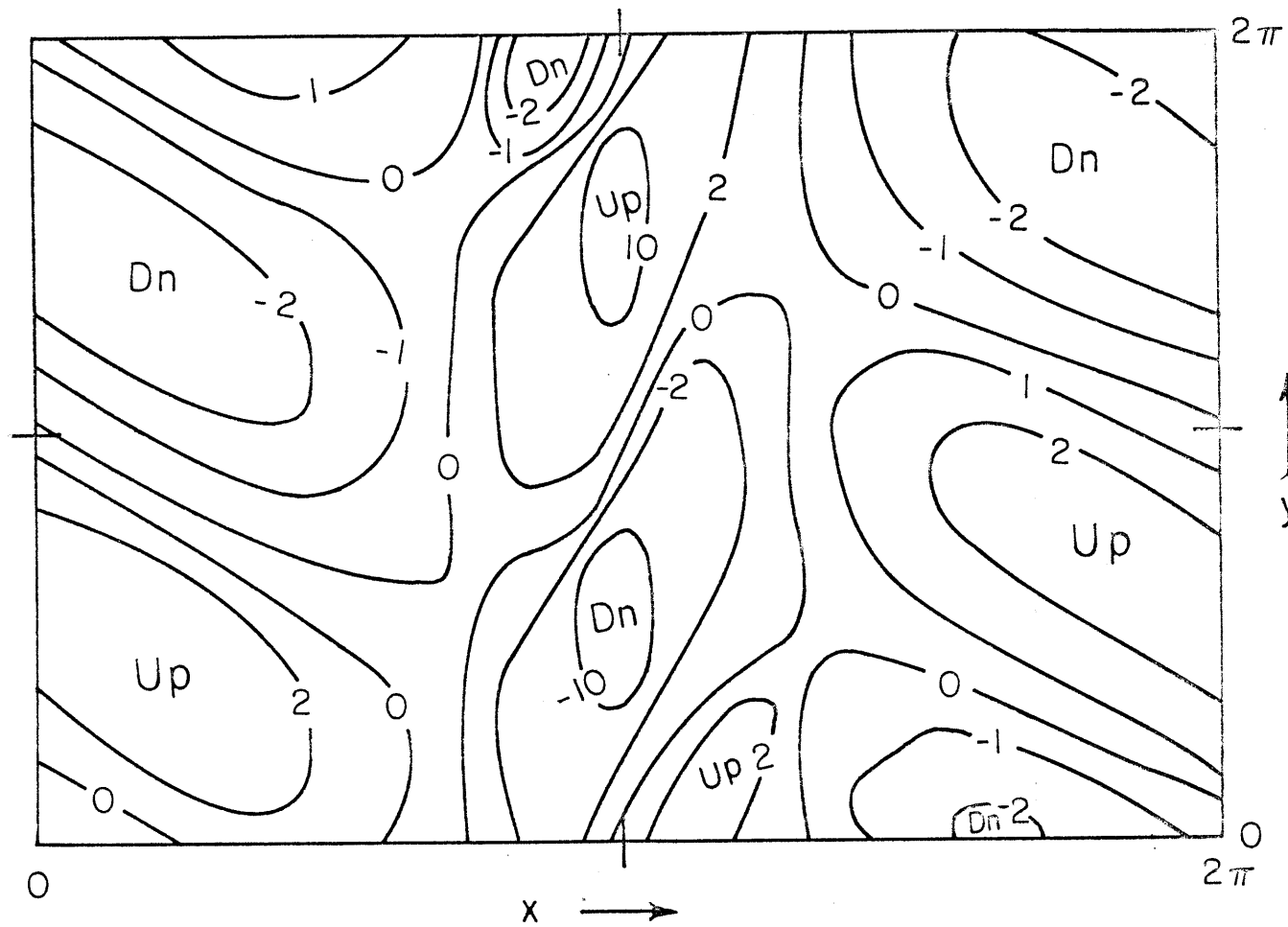Fig 8. Total potential temperature field at z = 0 in nondimensional units.

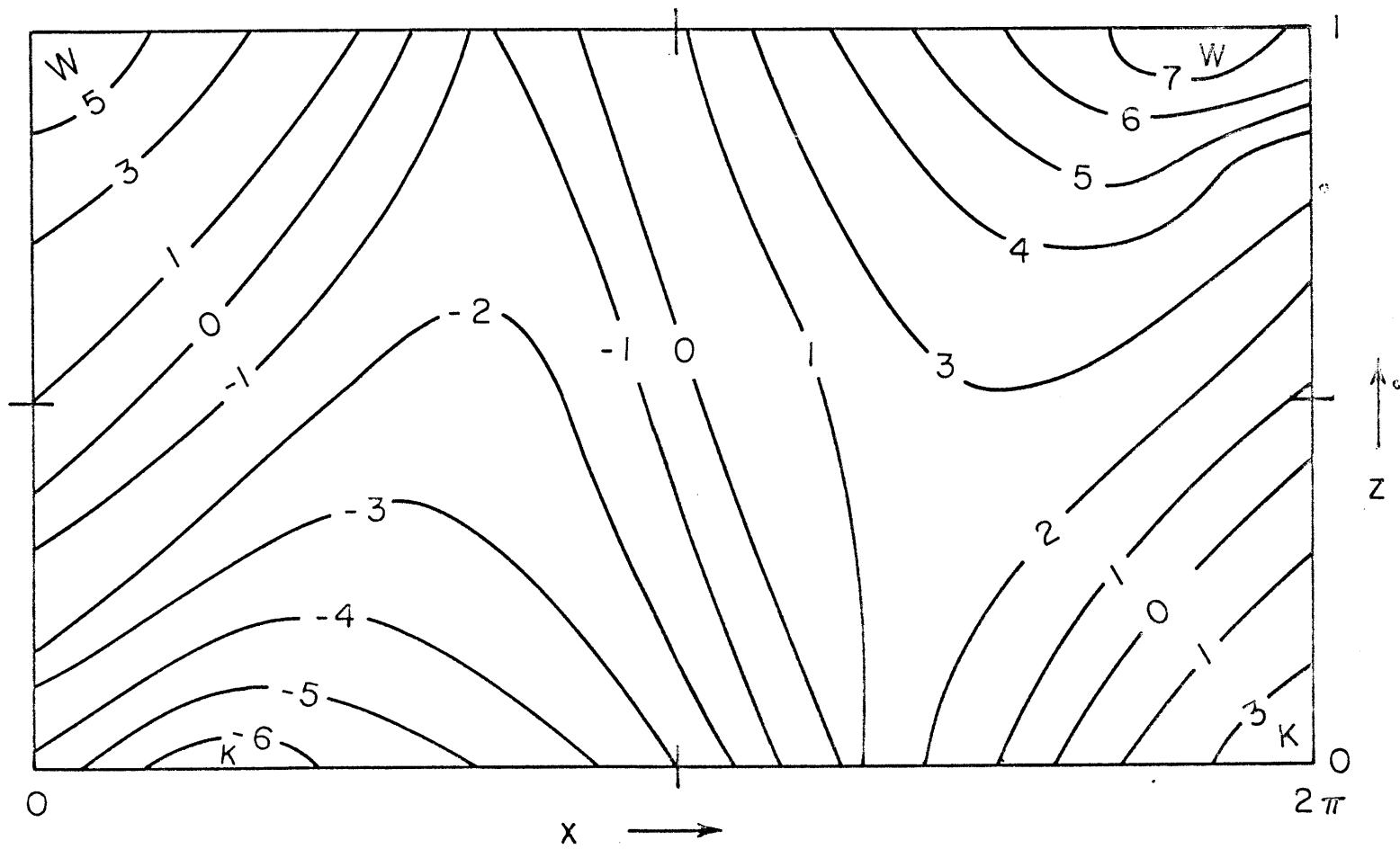Fig 9. Vertical velocity field at z = 1/2 in nondimensional units.

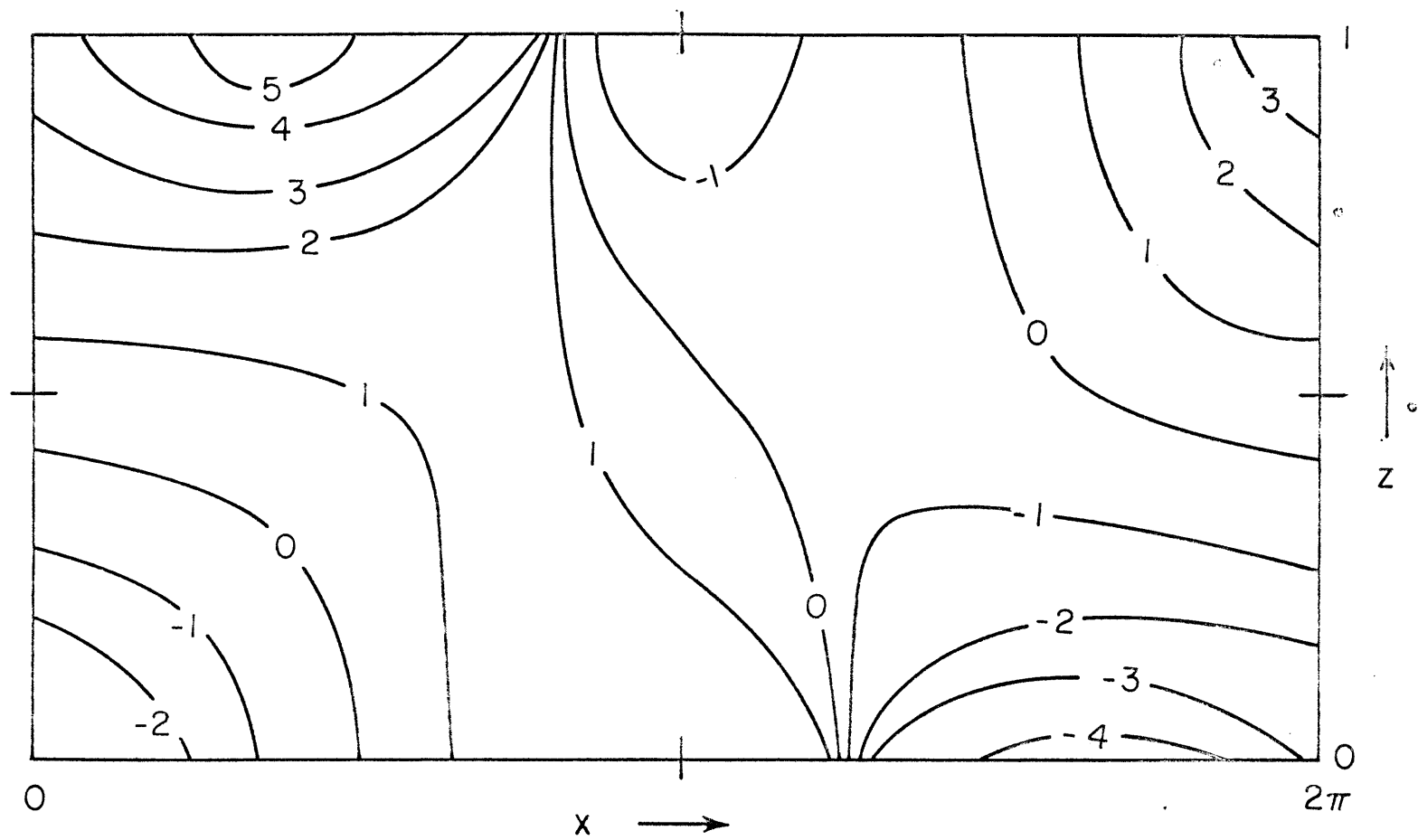Fig 10. Cross section of the total potential temperature field at y = 0 in nondimensional units.

Fig 11. Cross section of the total zonal velocity (with $\bar{u} = 1$ subtracted out) field at $y = 0$ in nondimensional units.
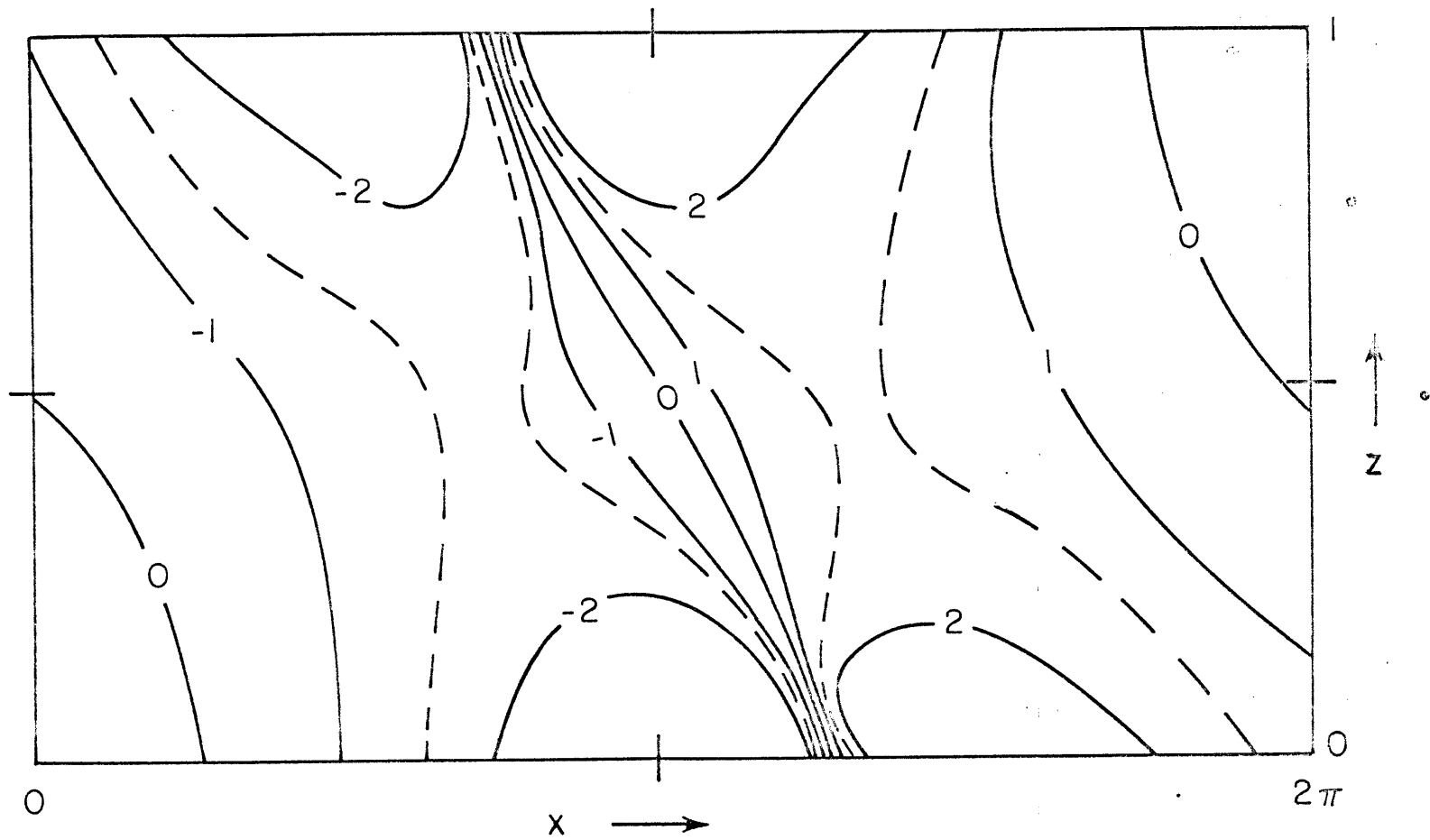
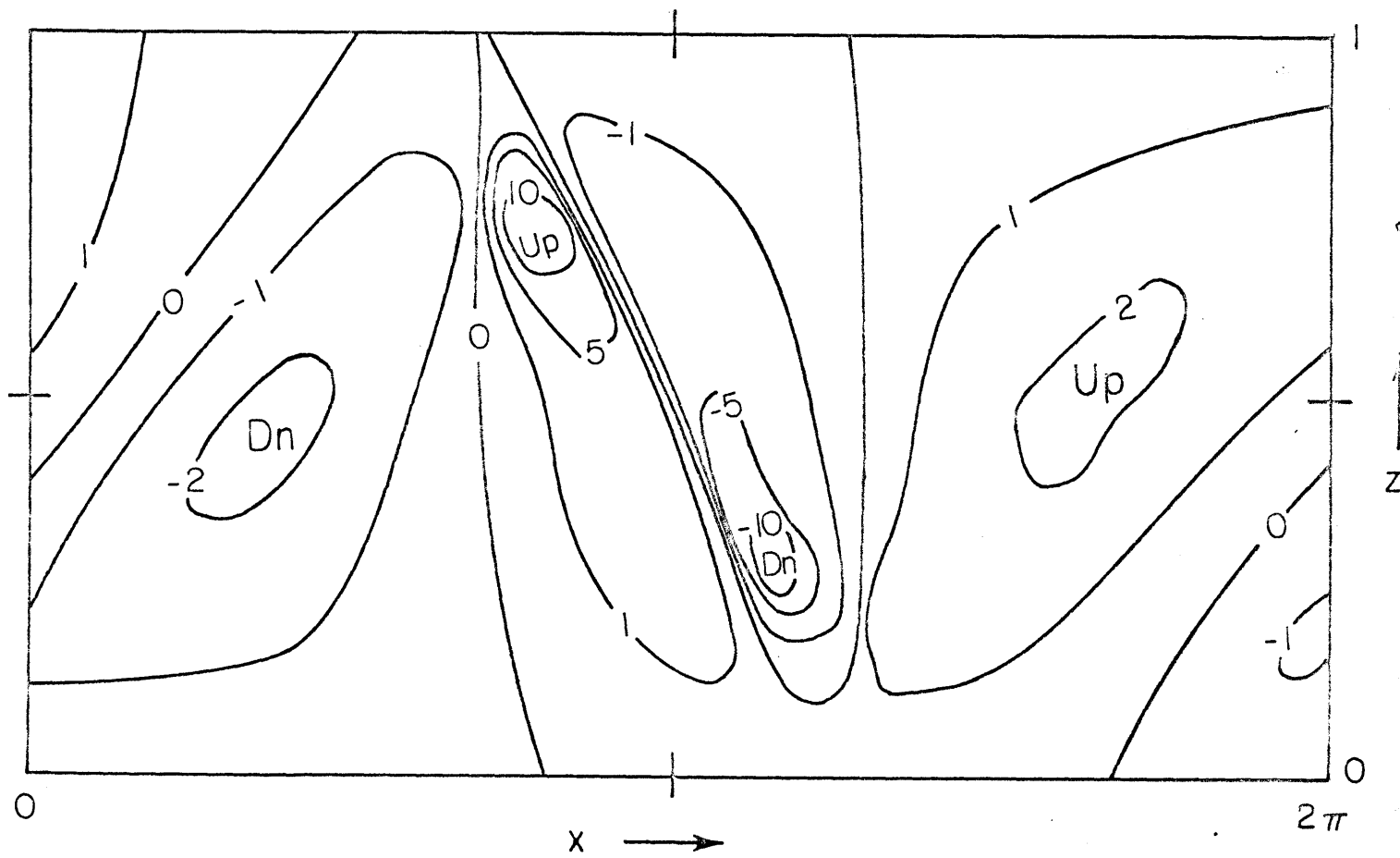Fig 12. Cross section of the total meridional velocity field at y = 0 in nondimensional units.

Fig 13. Cross section of the total vertical velocity field at y = 0 in nondimensional units.
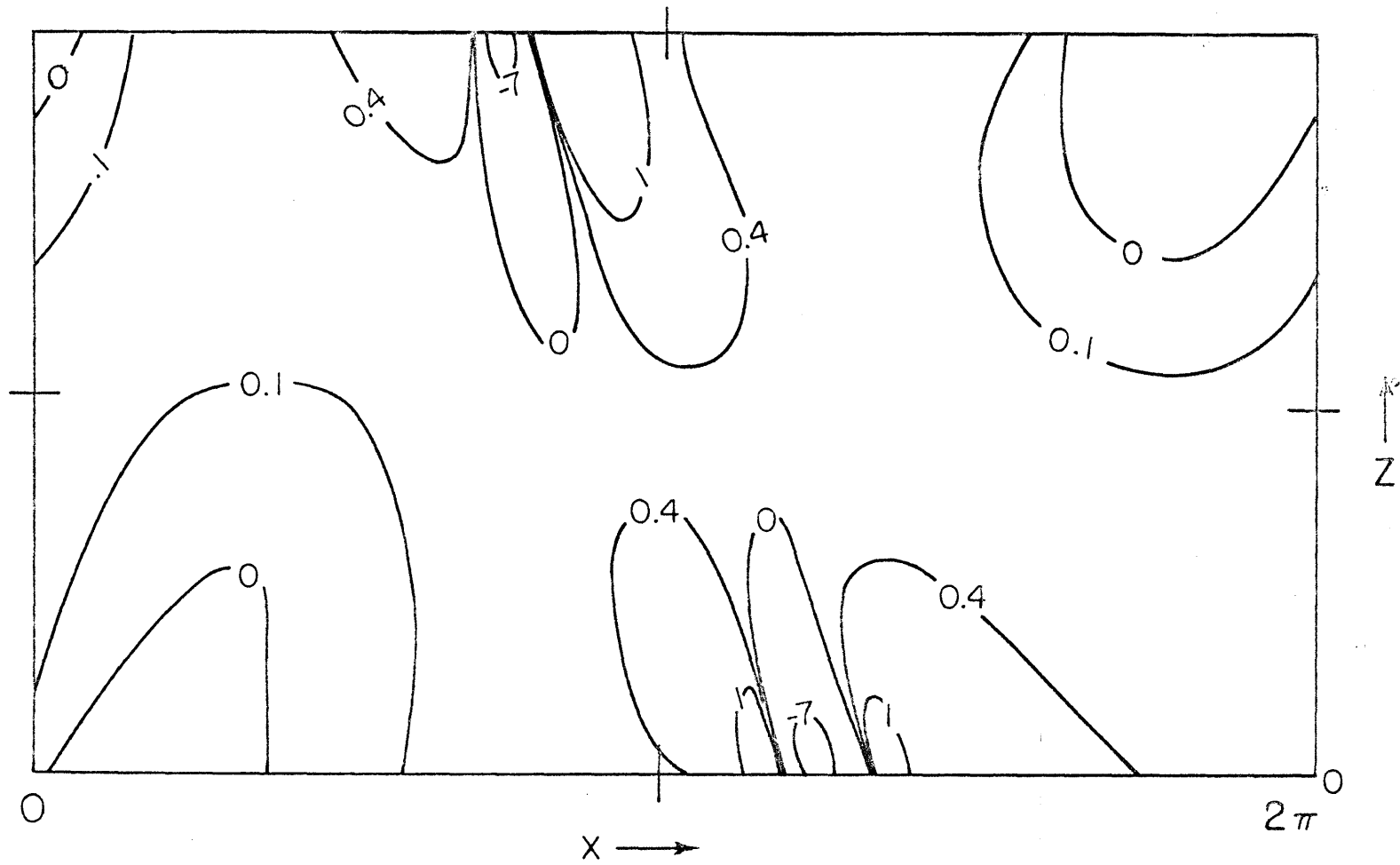
Fig 14. Relative vorticity field of the perturbations at y = 0
in nondimensional units.

10. <u>A</u> <u>synoptic</u> <u>example</u>: <u>a</u> <u>developing</u> <u>wave</u> <u>cyclone</u>.

In this section we shall apply the results obtained in the previous sections to a synoptic situation. In particular, we shall apply our solutions to a frontal cyclone development over the midwestern United States during 12-13 April 1964.

In Figs 15-17 we present the 500 mb surface heights, surface isobars, and vertical velocities for 00Z and 12Z 13 April 1964 as analyzed by Krishnamurti (1968) using conventional data and Tiros data.

In our analysis we shall associate the 00Z maps with our basic state. If we take the 500 mb surface to coincide with our $z = \frac{1}{2}$ level, the agreement between the trough depicted in Fig 2 and the smoothed 500 mb trough depicted in Fig 15 is excellant. At the surface there is a frontal surface which is essentially running north-south. The presence of the small surface lows indicate that the small perturbation, which will form the large-scale surface cyclone, is already present in the system.

In our model, we have taken $\bar{w} = 0$. Fig 17 shows that this is not quite accurate but compared with the vertical velocities that occur in the next 12 hr it is a good approximation. The strong sinking motion in the Colorado area is due to strong cold advection taking place in the Rocky Mountains area.

If we now associate the 12Z 13 April 1964 map with the flow field which results after the unstable perturbation has set in, then the pressure, temperature, and vertical velocity fields of the previous section can be used to explain the 12Z maps in Figs 15-17.

As Fig 15 shows, the trough has deepened in the northern Plains with the 540 dm contour coming down into Nebraska and a cutoff low has formed

over the Dakotas. Although we did not generate a cutoff low if Fig 6,

we do have a deepening of the trough in the region y = π/2 and 3π/2.

At the surface in Fig 16, a major, large-scale low has formed with

a cold front trailing southward and a warm front eastward from the low.

Comparing with Fig 8, we may associate the dividing line between the

cold air in the southwestern quadrant and the warm air in the south-

eastern quadrant with the cold front found in Fig 16. Likewise, the

dividing line between the warm air in the southeastern quadrant and the

cold air in the northeastern quadrant may be associated with the warm

front. We cannot, however, explain the small slice of warm air in the

northern half of Fig 8.

The most striking similarity between our model and this case study

is in the vertical velocities. A comparison of the predicted vertical

velocity field given by Fig 9 and the observed field given by Fig 17

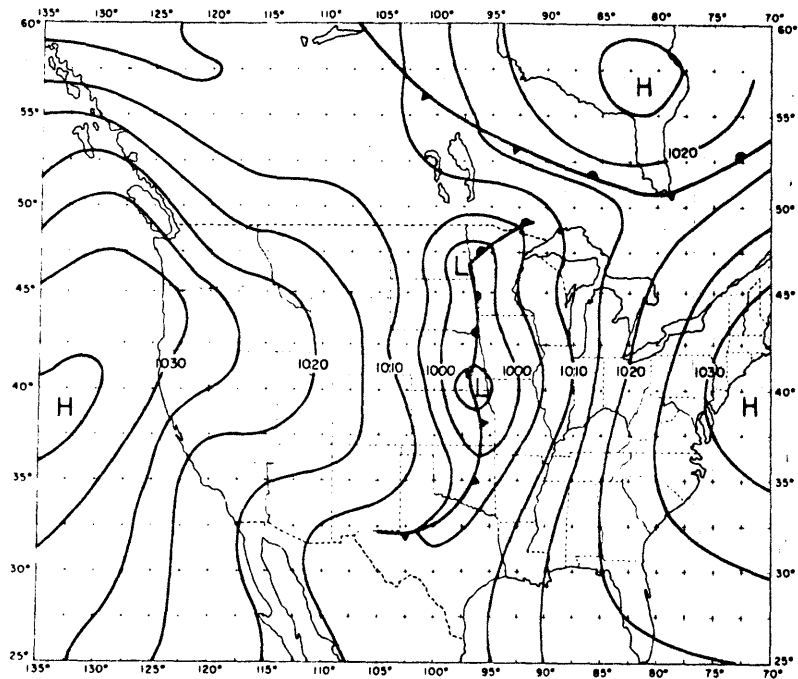shows that they are in good agreement with each other.
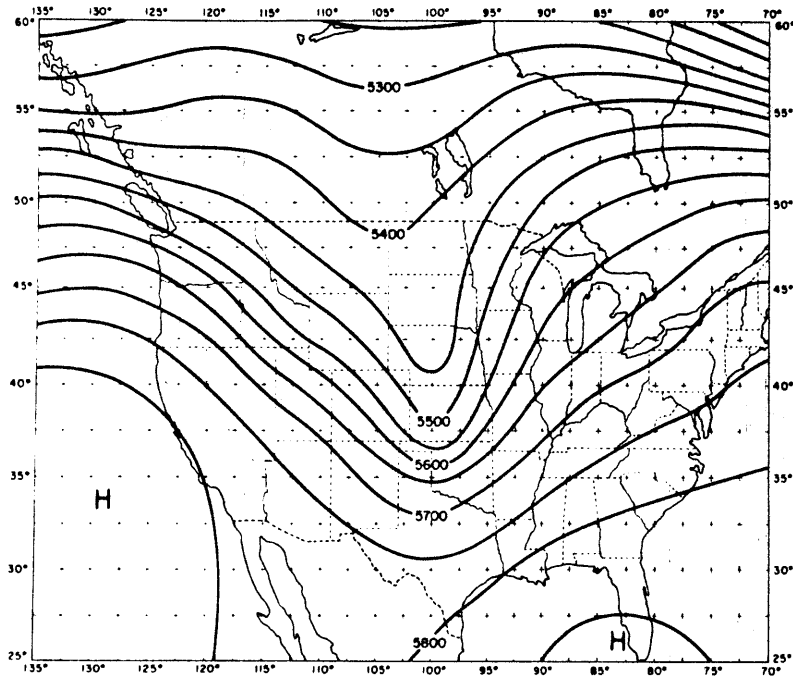
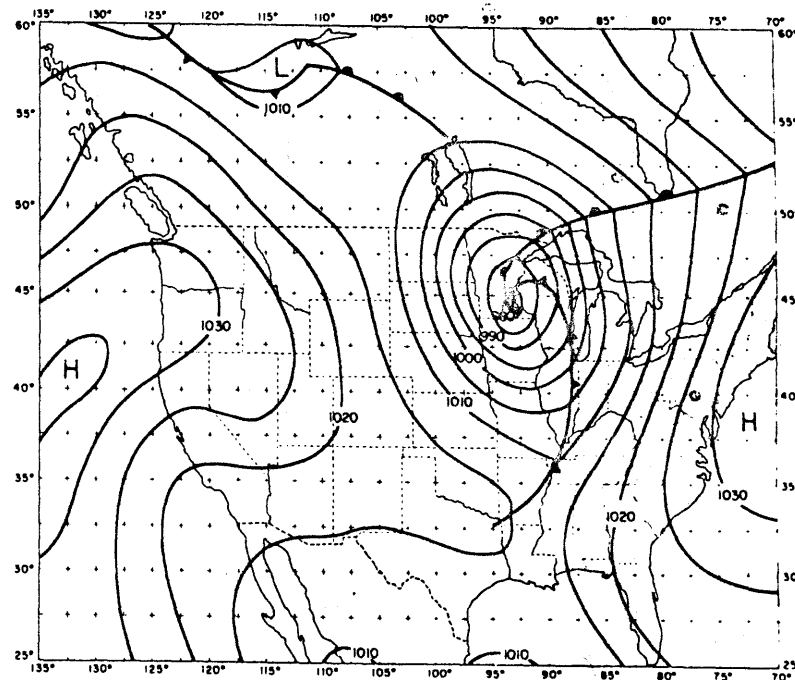500 MB  13 APRIL 1964  00Z
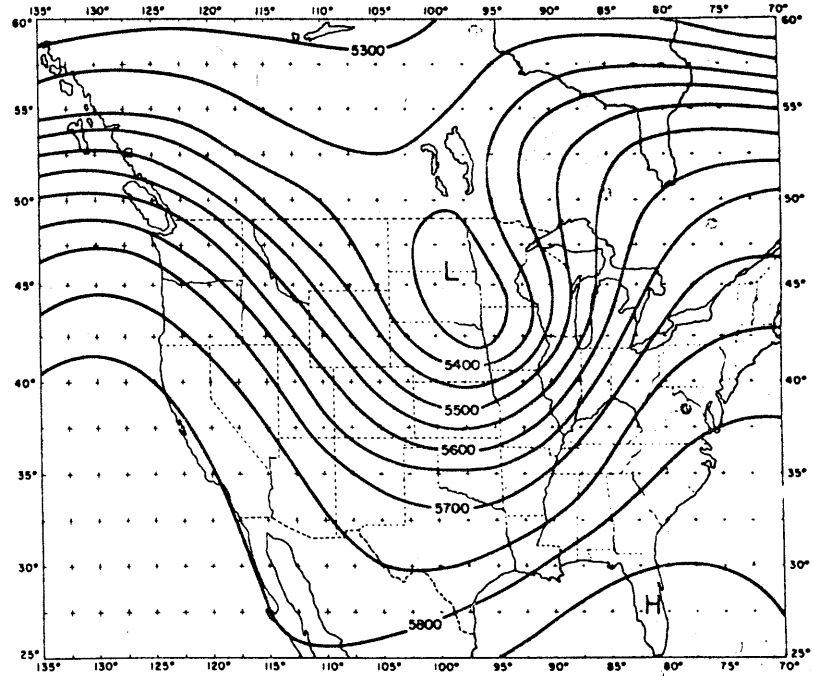
500 MB  13 APRIL 1964  12Z

Fig 15.   The 500 mb surface heights of continental United States at
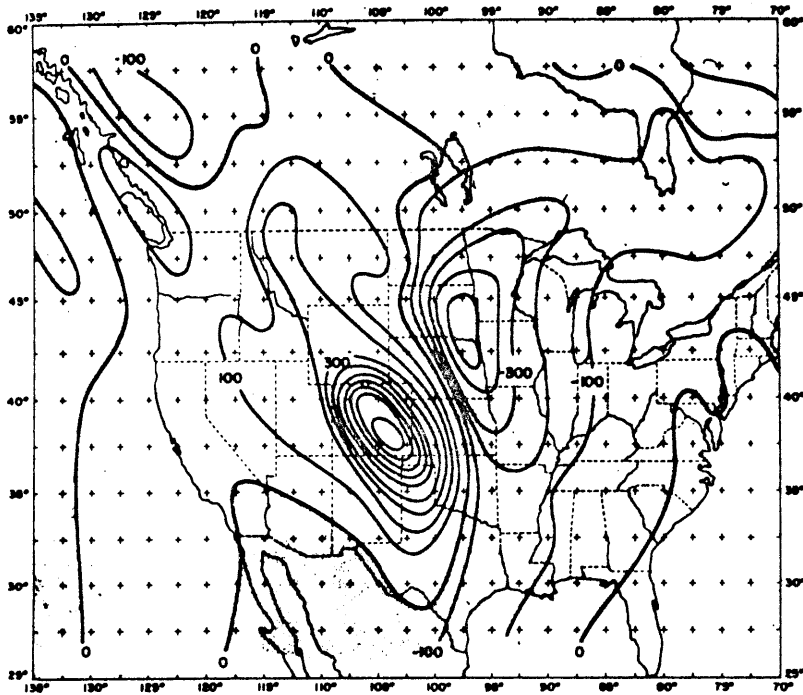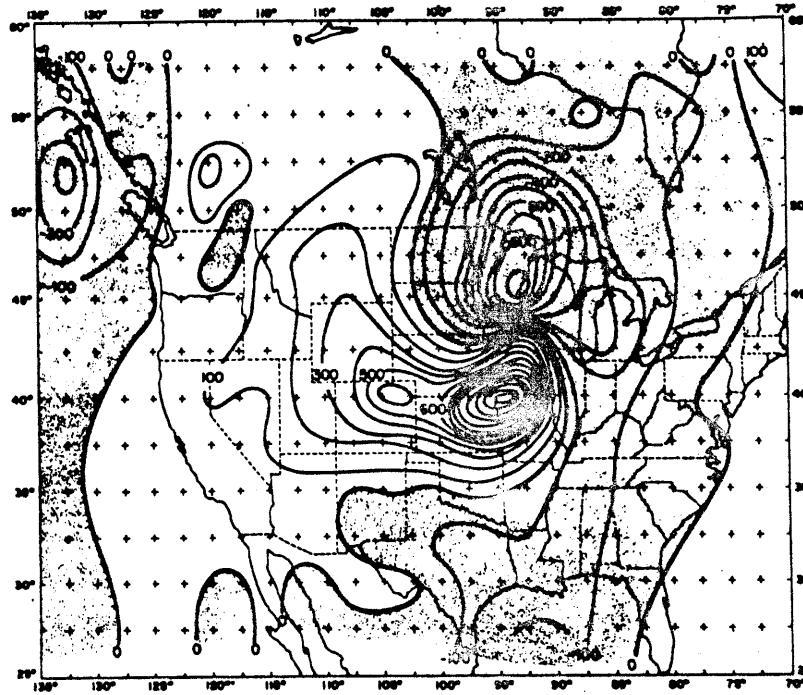          00Z and 12Z 13 April 1964.

SURFACE MAP 13 APRIL 1964 00Z

SURFACE MAP 13 APRIL 1964 12Z

Fig 16.   The surface isobars of continental United States at
00Z and 12Z 13 April 1964.

ω_L  500MB  13 APRIL 1964  00Z

ω_L  500MB  13 APRIL 1964  12Z

Fig 17.  Vertical velocities (in $10^{-5}$ mb/sec)
over continental United States at
00Z and 12Z 13 April 1964.

11. Conclusion.

In this thesis we have attempted to study frontal cyclogenesis primarily by analytical methods. Starting with the adiabatic, frictionless Boussinesq equations, we neglected high frequency phenemona and obtained the semigeostrophic equations (see Hoskins, 1975). Through the use of a coordinate transformation, the Eliassen coordinates, the governing equations were brought into a form which allowed a great deal of the nonlinearity to be eliminated.

As our time-independent basic state, we used a finite-amplitude solution, found by Hoskins and Bretherton (1972), to the semigeostrophic equations. Through the use of atmospheric statistics we showed that this finite-amplitude solution could be interpreted as a finite-amplitude Eady wave which had exhausted all of the zonal available potential energy. Fig 2 gives the pressure, velocity, and temperature fields of our basic state.

As a first attempt to study frontal cyclogenesis analytically, we adopted a constant potential vorticity model. We then perturbed the finite-amplitude baroclinic wave and obtained a set of perturbation equations. Although the exact perturbation equations could not be solved analytically, upon neglecting certain nonessential terms, analytical solutions were obtained and unstable modes were sought.

The baroclinic wave with its associated frontal surface was indeed found to be unstable to further perturbation. The most unstable perturbation was found to be stationary with respect to the zonal flow and derived its energy from both the available potential energy and kinetic energy of the finite-amplitude baroclinic wave. The character-

istic length scale of the most unstable disturbances was the Rossby

radius of deformation

The reason for these large-scale disturbances were shown to be

two-fold. In our model, we have taken the potential vorticity of

our basic state to be constant and the potential vorticity of the

perturbations to be zero. In the case of quasigeostrophic flow,

Charney and Stern (1962) have shown that there are two possible

sources of instability in a barotropic-baroclinic circumpolar vortex.

One of the sources of instability is the variations of the potential

temperature along the horizonta boundaries. We have this type of

instability in our model and it is associated with conventional

baroclinic instability. Another source of instability is due to

the vanishing of the meridional derivative of the potential vorticity

in an isentropic surfaces or the pseudopotential vorticity in a level

surface somewhere within the flow. In our problem, this would

correspond to a vanishing of the meridional derivative of the

basic state's potential vorticity somewhere within the flow. This

does not occur in our problem and has the consequence of excluding

Rayleigh instability in the flow.

This suggest, but does not prove, that the major frontal disturbances

are essentially baroclinic in nature and that only the smaller scale,

fast moving frontal waves are of the Rayleigh type.

In addition to performing stability calculations on the no zonal

shear case, caluclations were also made for the short wavelength cutoff

case. In this case, the boundary variation of the potential temperature

is such that instability cannot occur unless a zonal flow with shear

is present. However, we are not interested in conventional baroclinic

instability, modified somewhat due to the presence of the neutrally stable

Eady wave, and this analysis was not pursued further.

Finally, the first obvious modification to our analysis will be to

relax the constant potential vorticity constraint to allow the per-

turbations to have a nonconstant potential vorticity  and allow the

perturbation solution to have a nonzero $k_0$.

# REFERENCES

Bjerknes, J., 1937: Theorie der aussertropischen Zyklonenbildung. Meteor. Z., 54, 462-466.

___, and H. Solberg, 1922: Life cycle of cyclones and the polar front theory of atmospheric circulation. Geofys. Publ., 3, no. 1, 18 pp.

Bjerknes, V., J. Bjerknes, H. Solberg, and T. Bergeron, 1933: Physikalische Hydrodynamik. J. Springer, 797 pp.

Brown, J. A., 1969: A numerical investigation of hydrodynamic instability and energy conversions in the quasi-geostrophic atmosphere: Part I. J. Atmos. Sci., 26, 352-365.

Charney, J. G., 1947: The dynamics of long waves in a baroclinic westerly current. J. Meteor., 4, 135-163.

___, and M. E. Stern, 1962: On the stability of internal baroclinic jets in a rotating atmosphere. J. Atmos. Sci., 19, 159-173.

Duffy, D. G., 1975: The barotropic instability of Rossby wave motion: a reexamination. J. Atmos. Sci., 32, July issue.

Eliassen, A., 1949: The quasi-static equations of motion with pressure as independent variable. Geofys. Publ., 17, no. 3, 44 pp.

___, 1959: On the formation of fronts in the atmosphere. In The Atmosphere and the Sea in Motion, The Rockfeller Institute Press, 277-287.

Fjortoft, R., 1962: On the integration of a system of geostrophically balanced prognostic equations. Proc. Intern. Symp. Numerical Weather Prediction, Meteor. Soc. Japan, Tokyo, 153-159.

Gambo, K., 1970: The characteristic feature of medium-scale disturbances in the atmosphere (I) and (II). J. Meteor. Soc. Japan, Ser. II, 48, 173-184, 315-330.

Hoskins, B. J., 1975: The geostrophic momentum approximation and the semigeostrophic equations. J. Atmos. Sci., 32, 233-242.

___, and F. P. Bretherton, 1972: Atmospheric frontogenesis models: Mathematical formulation and solution. J. Atmos. Sci., 29, 11-37.

Krishnamurti, T. N., 1968: A study of a developing wave cyclone. Mon. Wea. Rev., 96, 208-217.

Nitta, T. and Y. Ogura, 1972: Numerical simulation of the development of the intermediate-scale cyclone in a moist model atmosphere. J. Atmos. Sci., 29, 1011-1024.

Nitta, T., 1964: On the development of the relatively small scale cyclone
due to the release of latent heat of condensation. J. Meteor. Soc.
Japan, Ser. II, 42, 260-276.

Orlanski, I., 1968: Instability of frontal waves. J. Atmos. Sci., 25,
178-200.

Oort, A. H., and E. M. Rasmusson, 1971: Atmospheric Circulation Statis-
tics. NOAA Professional Paper 5, 323 pp.

Palmen, E., and C. W. Newton, 1969: Atmospheric Circulation Systems:
Their Structure and Physical Interpretation. Academic Press, 603 pp.

Pedlosky, J., 1964: An initial value problem in the theory of baro-
clinic instability. Tellus, 16, 12-17.

Phillips, N. A., 1954: Energy transformations and meridional circulations
associated with simple baroclinic waves in a two-level, quasi-geostro-
phic model. Tellus, 6, 273-286.

Solberg, H., 1928: Integrationen der atmosphärischen Störungsgleichungen.
Geofys. Publ., 5, no. 9, 120 pp.

Stone, P. H,, 1966: On non-geostrophic baroclinic instability. J. Atmos.
Sci., 23, 390-400.

Tokioka, T., 1970: Non-geostrophic and non-hydrostatic instability of a
baroclinic fluid. J. Meteor. Soc. Japan, Ser. II, 48, 503-520.

____, 1971: Supplement to non-geostrophic and non-hydrostatic stability
of a baroclinic fluid and medium-scale disturbances on the fronts.
J. Meteor. Soc. Japan, Ser. II, 49, 129-132.

Wilkinson, J. H. et al, 1971: Handbook for Automatic Computation:
Volume II. Springer-Verlag, 439 pp.

Williams, R. T., 1967: Atmospheric frontogenesis: a numerical experiment.
J. Atmos. Sci., 24, 627-641.

BIOGRAPHICAL NOTE

The author was born on 9 July 1949 in Meadville, PA. He was reared in Ohio, Pennsylvania, Illinois, and Texas. In 1971, he received a B. S. in geophysics as an undergraduate scholar from Case Institute of Technology. He enrolled at M.I.T. in September 1971, where he has been supported by a NDEA fellowship and a research assistantship.

He is currently assigned to the U. S. Air Force's Global Weather Central at Offutt AFB.